Figure 2. Dot plot of short read coverage (Cov.) at every nucleotide for the 8 segments of A/Nagano/RC1-L/2009(H1N1). To obtain the consensus sequences for the respective 8 segments, 40-mer short reads were aligned to the complete segment sequences of A/Tronto/T0106/2009(H1N1) (gb|CY045951.1 – .8). Short read sequencing was performed using total RNA including human RNA, and also vRNA, cRNA, and mRNA from influenza A virus; thus, coverage bias was detected throughout the segments, but the average coverage (AC) is likely to be similar at approximately ×200 or more. The horizontal red arrows show the location of the contigs obtained by *de novo* assembly, as shown in Table 1.
doi:10.1371/journal.pone.0010256.g002

in the human upper airway [22], while it apparently shows minimal contact with α2-3 sialylated glycans present in the human lower respiratory tract [23]. Indeed, the recombinant A/H1N1/2009 HA has been characterized to exhibit lower binding to the alveolar tissue of the lower respiratory tract [17]. However, we previously detected abundant viral nucleoprotein of A/Nagano/

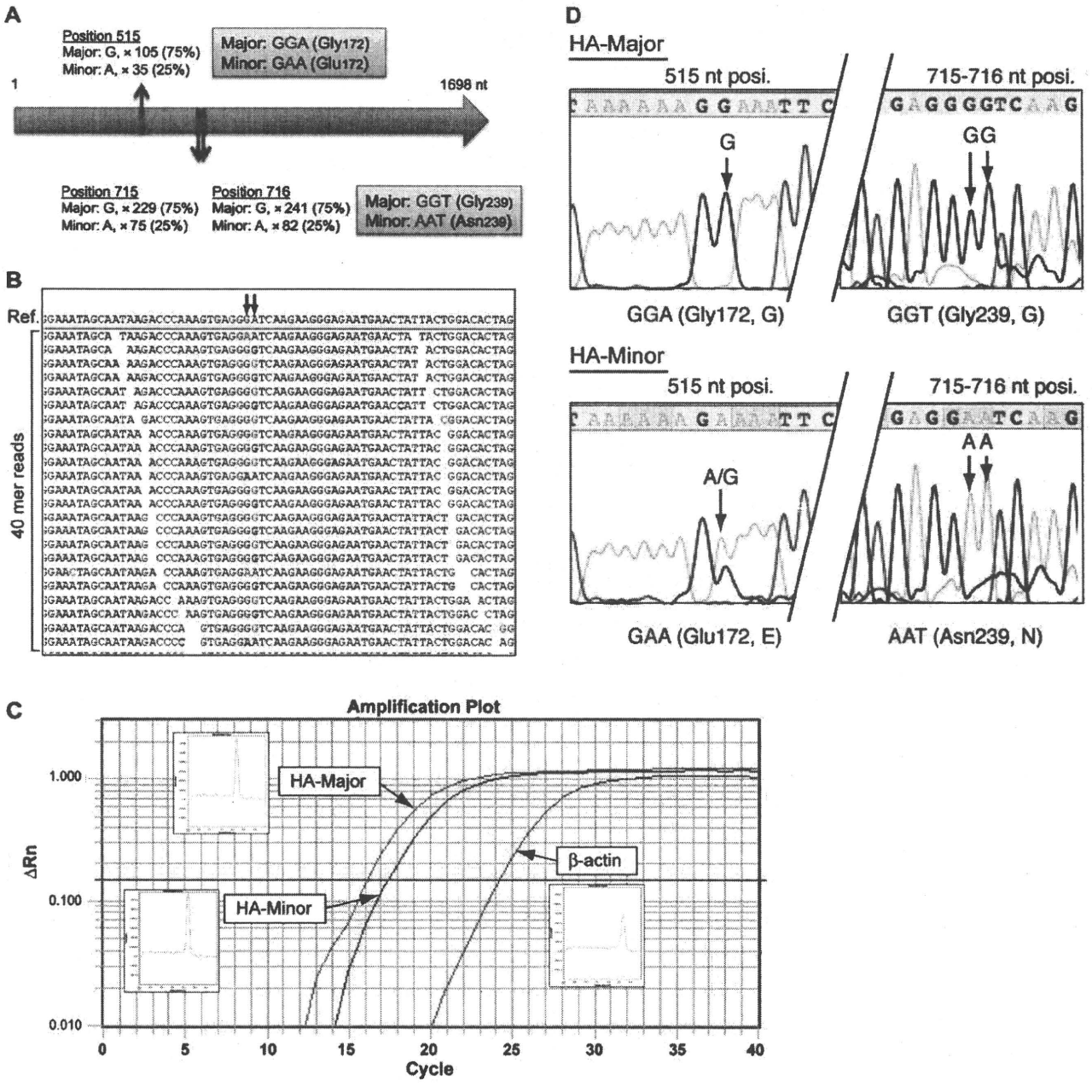

Figure 3. Genetic variations of the HA nucleotide sequence. (**A**) Schematic representation of 3 nucleotide variations (positions 515, 715, and 716 nt) in the HA coding nucleotide sequence. Three variations were classified as Major (75% appearance) or Minor (25% appearance) by read coverage (×), and the coding amino acids are also shown. (**B**) Arrows indicate positions 715 and 716 nt of the HA sequence, and the alignment image of the 40-mer reads. Nucleotides shown in red are the mismatches to the reference sequence of A/Tronto/T0106/2009(H1N1). Every read suggested that either the GGT or AAT sequence was present, but not the GAT or AGT sequence. (**C**) An amplification plot for HA-specific qRT-PCR. (**D**) Validation of genetic variation by Sanger capillary sequencing. HA-Major or HA-Minor PCR products were obtained by qRT-PCR using HA-Major- or HA-Minor-specific PCR primers. HA-Major PCR product shows G nucleotides at positions 515, 715, and 716 nt, while HA-Minor shows A nucleotides.
doi:10.1371/journal.pone.0010256.g003

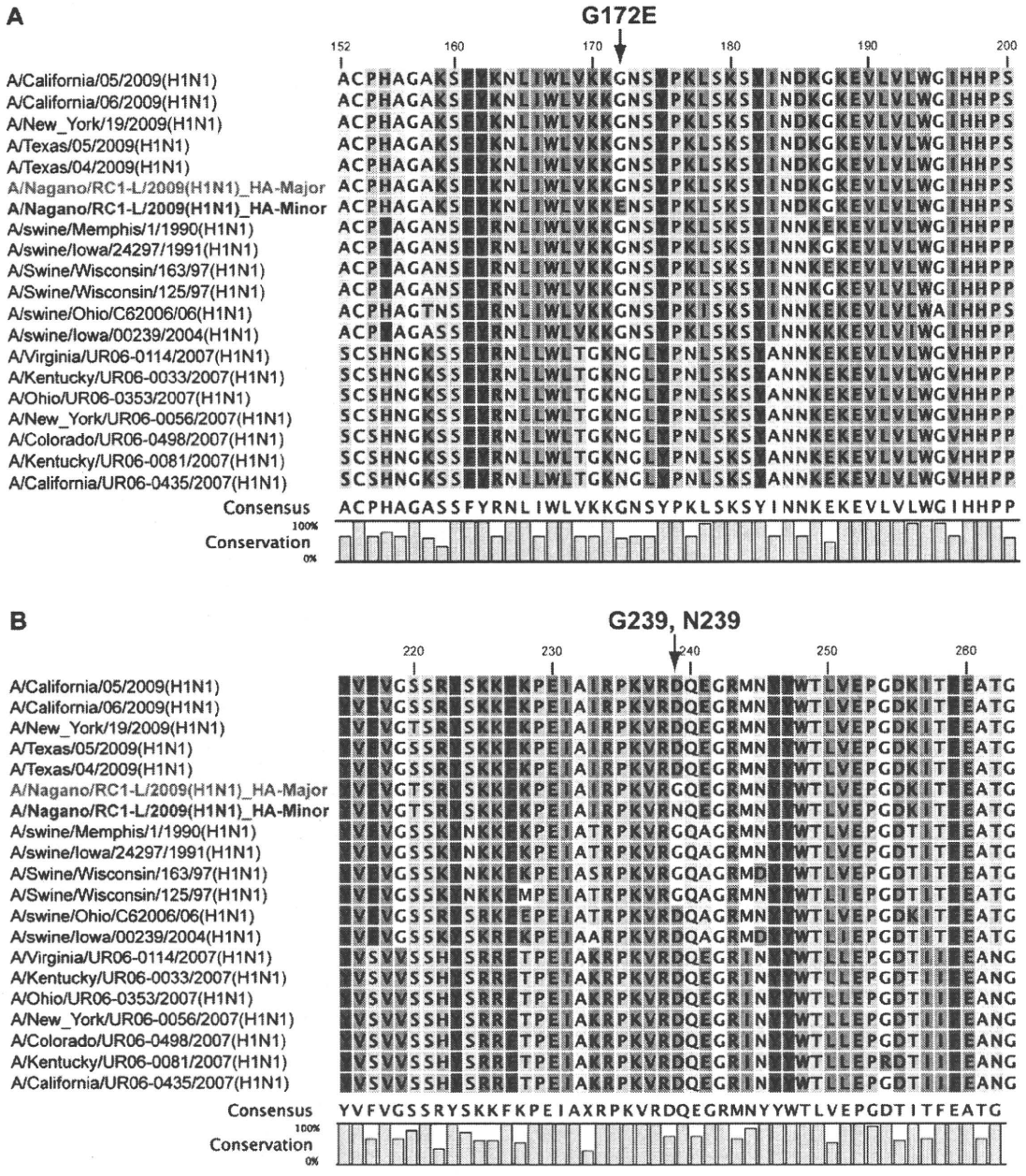

Figure 4. Alignment of HA amino acid sequences in influenza A virus around the identified mutations in A/Nagano/RC1-L/2009(H1N1). (**A**) Genetic variation at position 515 nt causes the amino acid substitution $Gly_{172}Glu$; HA-Major: Gly172, HA-Minor: Glu172. (**B**) Genetic variation at position 715 and 716 nt causes the amino acid substitution $Gly_{239}Asn$; HA-Major: Gly239, HA-Minor: Asn239.
doi:10.1371/journal.pone.0010256.g004

RC1-L/2009(H1N1) in pneumocytes expressing α2-3 sialylated glycans in autopsy lung tissue sections [15], suggesting that the above substitutions could affect the binding affinity to both types of sialylated glycans.

Very suggestive reports predicted the possible future antigenic drift of A/H1N1/2009 viruses from viral sequence and structural comparative analyses [11,12]. Prior to the initiation of the current study (September 2009), Igarashi *et al.* predicted possible substitutions and these included the two amino acid substitutions presented here ($Gly_{172}Glu$ and $Asp_{239}Gly$) [11]. Furthermore, Shen *et al.* suggested that host-driven antigenic drift based on evolutionary trends appeared to favor Asp239 (corresponding to Asp225 in the mature HA) in swine HAs and the 1918 pandemic, while Asp204 (corresponding to Asp190 in the mature HA) was favored in seasonal H1N1 HAs [12]. These predictions are very attractive and our experiments demonstrated one of them *a posteriori*. Furthermore, recent study has shown that receptor-binding avidity can influence antigenic drift [24]. HA antigenic sites Sa is the membrane proximal region, therefore, the identified variations on both Sa and Ca2 might contribute to the alteration of antigenicity and receptor-binding avidity by synergistic effect. The newly identified Asn239 substitution could be a probable candidate for further investigation of the manner of viral binding to sialic acid on the host receptors.

In conclusion, this study demonstrated that *de novo* sequencing can comprehensively detect pathogens, and such in-depth

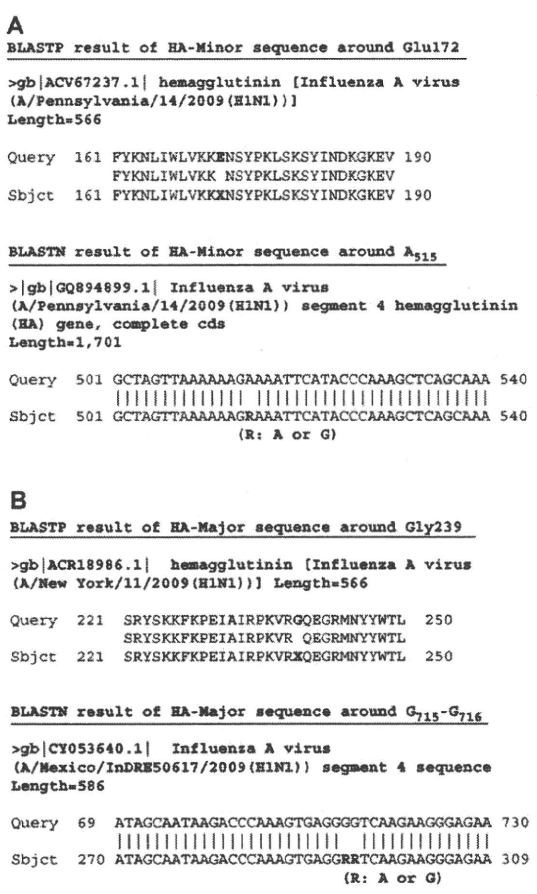

Figure 5. BLAST homology search of the HA sequences against the nr or nt databases. (**A**) Glu172 of HA-Minor. (**B**) Gly239 of HA-Major. R: A or G.
doi:10.1371/journal.pone.0010256.g005

investigation facilitates the identification of influenza A viral heterogeneity during infection. The possibility of mixed infections with variants remains to be elucidated in this case, but worldwide sequencing efforts suggest that quasispecies of the A/H1N1/2009 virus evidently appear and are observed. To better characterize the currently emerging A/H1N1/2009 virus and prevent worse pandemics in the near future, unbiased *de novo* sequencing techniques will be indispensable for the primary investigations of emerging infectious diseases.

Materials and Methods

Ethics Statement

The study protocol was approved by the institutional medical ethical committee, National Institute of Infectious Diseases, Japan (Approval No.236), and the study was conducted according to the Declaration of Helsinki Principles. In the autopsy case, a written consent for autopsy was obtained from relatives.

Total RNA and cDNA preparation from autopsy human lung

Information for the patient was previously reported [15]. Briefly, in August 2009, a 33-year-old male patient with chronic heart failure due to dilated cardiomyopathy, mild diabetes mellitus, atopic dermatitis, asthma, and obesity (BMI: 38) died from respiratory failure and multiple organ dysfunction syndrome. A diagnosis of pandemic influenza A virus (A/H1N1/2009) infection was determined using RT-PCR testing in a clinical laboratory. Total RNA was prepared from a 5-mm cube of the autopsy lung tissue using ISOGEN (NipponGene, Japan), followed by Ambion TurboDNase treatment (Ambion, Austin, TX USA). Double-stranded cDNA was prepared from 5 μg of total RNA using the random priming method with SuperScript Choice System for cDNA synthesis (Invitrogen, Carlsbad, CA, USA). cDNA was purified using a QIAquick PCR Purification kit (QIAGEN, Hilden, Germany).

Short-read DNA sequencing using the Illumina Genome Analyzer II

An approximately 300-bp length cDNA library was prepared using a genomic DNA sample prep kit (Illumina, San Diego, CA, USA), and DNA clusters were generated on a slide using a Cluster Generation kit (ver. 2) on an Illumina cluster station (Illumina), according to the manufacturer's instructions. To obtain $\sim 1.0 \times 10^7$ clusters for one lane, the general procedure as described in the standard recipe (Illumina) was performed as follows: template hybridization, isothermal amplification, linearization, blocking, denaturation, and hybridization of the sequencing primer (Illumina). All sequencing runs for 40 mers were performed with GA II using the Illumina Sequencing kit (ver. 3). Fluorescent images were analyzed using the Illumina base-calling pipeline 1.4.0 to obtain FASTQ formatted sequence data.

Homology search analysis

The obtained DNA sequences were investigated using a BLAST search as shown in Fig. 1A. The results of the BLASTN search were analyzed and visualized using MEGAN v3.7.4 [25] with the following parameters: minimum support, 5; minimum score, 35.0.

de novo assembly of short reads

Prior to *de novo* assembly, all obtained 40-mer reads were trimmed based on the *phred* quality value obtained using the Euler-SR *qualitytrimmer* command [26]. Such trimmed read sequences were assembled using Velvet v0.7.55 [27] or Euler-SR v1.0 [26] with the default parameters (Velvet: hash length, 25; Euler-SR: vertex size, 25).

Read mapping

To obtain consensus sequences for the respective 8 segments of influenza A virus, 40-mer short reads were aligned to A/Tronto/T0106/2009(H1N1) sequences (gb|CY045951.1 – .8) as reference sequences with Maq software (ver. 0.7.1) [28] using the *easyrun* Perl-command. The consensus sequences were extracted as a "cns.fq" file for each segment, and deposited in the DNA Data Bank of Japan (DDBJ; accession numbers: AB538386 to AB538393 for the 8 segments of A/Nagano/RC1-L/2009(H1N1), and AB538394 for segment 4 encoding the HA-Minor sequence). Read coverage at every nucleotide was obtained using Maq software (ver. 0.7.1) with the *pileup* command. Read alignment for the validation of SNPs was performed using the MapView graphical alignment viewer [29].

qRT-PCR analysis

qRT-PCR was performed using 100 ng of total RNA, HA variant-specific primers (forward common primer: pdmFlu09-HA-F, 5′–CGAACAAAGGTGTAACGGCAGCAT–3′; HA-Major-specific reverse primer: pdmFlu-HA-R_Major, 5′–ATAGTTCATTCTCCCTTCTTGACC–3′; HA-Minor-specific reverse primer: 5′–ATAGTTCATTCTCCCTTCTTGATT–3′), and

the SuperScript III Platinum SYBR Green One-Step qRT-PCR kit with ROX (Invitrogen), and analyzed using the ABI PRISM 7900HT Real-time PCR System (Applied Biosystems, Foster City, CA, USA). The following qRT-PCR program was used: RT reaction, 50°C for 3 min; initial denaturation, 95°C for 5 min; 2 steps of amplification (×40 cycles), 95°C for 15 sec and 60°C for 30 sec. The human β-actin gene was used as the internal control. PCR products were resolved by 5% polyacrylamide gel electrophoresis, followed by Sanger sequencing using the BigDye Terminator v3.1 Cycle Sequencing kit (Applied Biosystems).

Virus isolation

The A/H1N1/2009 virus was isolated from MDCK cells passaged once with trypsin.

Supporting Information

Text S1 Fastq file of the 40-mer short reads with similarity to influenza A virus extracted from whole obtained short reads.
Found at: doi:10.1371/journal.pone.0010256.s001 (11.19 MB PDF)

Text S2 De novo assembly of the influenza A virus using Euler-SR v1.0 [26] with the default parameters (vertex size, 25).
Found at: doi:10.1371/journal.pone.0010256.s002 (0.04 MB RTF)

Acknowledgments

We thank Tadahito Kanda for valuable suggestions.

Author Contributions

Conceived and designed the experiments: MK TS. Performed the experiments: MK HK TS YS. Analyzed the data: MK HK TS HH. Contributed reagents/materials/analysis tools: HK NN MT AA MT YA SH MW TS. Wrote the paper: MK.

References

1. Dawood FS, Jain S, Finelli L, Shaw MW, Lindstrom S, et al. (2009) Emergence of a novel swine-origin influenza A (H1N1) virus in humans. N Engl J Med 360: 2605–2615.
2. Gill JR, Sheng ZM, Ely SF, Guinee DG, Beasley MB, et al. (2010) Pulmonary pathologic findings of fatal 2009 pandemic influenza A/H1N1 viral infections. Arch Pathol Lab Med 134: 235–243.
3. Ghedin E, Sengamalay NA, Shumway M, Zaborsky J, Feldblyum T, et al. (2005) Large-scale sequencing of human influenza reveals the dynamic nature of viral genome evolution. Nature 437: 1162–1166.
4. Kilbourne ED (2006) Influenza pandemics of the 20th century. Emerg Infect Dis 12: 9–14.
5. Nelson MI, Viboud C, Simonsen L, Bennett RT, Griesemer SB, et al. (2008) Multiple reassortment events in the evolutionary history of H1N1 influenza A virus since 1918. PLoS Pathog 4: e1000012.
6. Knossow M, Skehel JJ (2006) Variation and infectivity neutralization in influenza. Immunology 119: 1–7.
7. Air GM, Laver WG, Webster RG (1987) Antigenic variation in influenza viruses. Contrib Microbiol Immunol 8: 20–59.
8. Caton AJ, Brownlee GG, Yewdell JW, Gerhard W (1982) The antigenic structure of the influenza virus A/PR/8/34 hemagglutinin (H1 subtype). Cell 31: 417–427.
9. Bui HH, Peters B, Assarsson E, Mbawuike I, Sette A (2007) Ab and T cell epitopes of influenza A virus, knowledge and opportunities. Proc Natl Acad Sci U S A 104: 246–251.
10. Squires B, Macken C, Garcia-Sastre A, Godbole S, Noronha J, et al. (2008) BioHealthBase: informatics support in the elucidation of influenza virus host pathogen interactions and virulence. Nucleic Acids Res 36: D497–503.
11. Igarashi M, Ito K, Yoshida R, Tomabechi D, Kida H, et al. (2010) Predicting the antigenic structure of the pandemic (H1N1) 2009 influenza virus hemagglutinin. PLoS One 5: e8553.
12. Shen J, Ma J, Wang Q (2009) Evolutionary trends of A(H1N1) influenza virus hemagglutinin since 1918. PLoS One 4: e7789.
13. Nakamura S, Yang CS, Sakon N, Ueda M, Tougan T, et al. (2009) Direct metagenomic detection of viral pathogens in nasal and fecal specimens using an unbiased high-throughput sequencing approach. PLoS One 4: e4219.
14. Ramakrishnan MA, Tu ZJ, Singh S, Chockalingam AK, Gramer MR, et al. (2009) The feasibility of using high resolution genome sequencing of influenza a viruses to detect mixed infections and quasispecies. PLoS One 4: e7105.
15. Nakajima N, Hata S, Sato Y, Tobiume M, Katano H, et al. (2010) The first autopsy case of pandemic influenza (A/H1N1pdm) virus infection in Japan: Detection of high copy number of the virus in type II alveolar epithelial cells by pathological and virological examination. Jpn J Infect Dis 63: 67–71.
16. Palacios G, Hornig M, Cisterna D, Savji N, Bussetti AV, et al. (2009) *Streptococcus pneumoniae* coinfection is correlated with the severity of H1N1 pandemic influenza. PLoS One 4: e8540.
17. Maines TR, Jayaraman A, Belser JA, Wadford DA, Pappas C, et al. (2009) Transmission and pathogenesis of swine-origin 2009 A(H1N1) influenza viruses in ferrets and mice. Science 325: 484–487.
18. Louie J, Jean C, Chen T-H, Park S, Ueki R, et al. (2009) Bacterial coinfections in lung tissue specimens from fatal cases of 2009 pandemic influenza A (H1N1) - United States, May-August 2009. MMWR Morb Mortal Wkly Rep 58: 1071–1074.
19. Greenbaum JA, Kotturi MF, Kim Y, Oseroff C, Vaughan K, et al. (2009) Pre-existing immunity against swine-origin H1N1 influenza viruses in the general human population. Proc Natl Acad Sci U S A 106: 20365–20370.
20. Gamblin SJ, Haire LF, Russell RJ, Stevens DJ, Xiao B, et al. (2004) The structure and receptor binding properties of the 1918 influenza hemagglutinin. Science 303: 1838–1842.
21. Soundararajan V, Tharakaraman K, Raman R, Raguram S, Shriver Z, et al. (2009) Extrapolating from sequence–the 2009 H1N1 'swine' influenza virus. Nat Biotechnol 27: 510–513.
22. Chandrasekaran A, Srinivasan A, Raman R, Viswanathan K, Raguram S, et al. (2008) Glycan topology determines human adaptation of avian H5N1 virus hemagglutinin. Nat Biotechnol 26: 107–113.
23. Shinya K, Ebina M, Yamada S, Ono M, Kasai N, et al. (2006) Avian flu: influenza virus receptors in the human airway. Nature 440: 435–436.
24. Hensley SE, Das SR, Bailey AL, Schmidt LM, Hickman HD, et al. (2009) Hemagglutinin receptor binding avidity drives influenza A virus antigenic drift. Science 326: 734–736.
25. Mitra S, Klar B, Huson DH (2009) Visual and statistical comparison of metagenomes. Bioinformatics 25: 1849–1855.
26. Chaisson MJ, Pevzner PA (2008) Short read fragment assembly of bacterial genomes. Genome Res 18: 324–330.
27. Zerbino DR, Birney E (2008) Velvet: algorithms for de novo short read assembly using de Bruijn graphs. Genome Res 18: 821–829.
28. Li H, Ruan J, Durbin R (2008) Mapping short DNA sequencing reads and calling variants using mapping quality scores. Genome Res 18: 1851–1858.
29. Bao H, Guo H, Wang J, Zhou R, Lu X, et al. (2009) MapView: visualization of short reads alignment on a desktop computer. Bioinformatics 25: 1554–1555.

Virology 398 (2010) 273–279

Contents lists available at ScienceDirect

Virology

journal homepage: www.elsevier.com/locate/yviro

Nuclear localization of Merkel cell polyomavirus large T antigen in Merkel cell carcinoma

Tomoyuki Nakamura [a], Yuko Sato [a], Daisuke Watanabe [b], Hideki Ito [c], Nozomi Shimonohara [a], Takahiro Tsuji [a], Noriko Nakajima [a], Yoshio Suzuki [d], Koma Matsuo [c], Hidemi Nakagawa [c], Tetsutaro Sata [a], Harutaka Katano [a,*]

[a] Department of Pathology, National Institute of Infectious Diseases, 1-23-1 Toyama, Shinjuku, Tokyo 162-8640, Japan
[b] Department of Dermatology, Aichi Medical University, Nagakute, Aichi 480-1195, Japan
[c] Department of Dermatology, Jikei University School of Medicine, Minato, Tokyo 105-8461, Japan
[d] Department of Pathology, Asahi General Hospital, Asahi, Chiba 289-2511, Japan

ARTICLE INFO

Article history:
Received 13 October 2009
Returned to author for revision
10 November 2009
Accepted 17 December 2009
Available online 13 January 2010

Keywords:
Merkel cell polyomavirus
Large T antigen
Merkel cell carcinoma
Nuclear localization signal
Mutation

ABSTRACT

To clarify whether mutations in the large T gene encoded by Merkel cell polyomavirus affect the expression and function of large T antigen in Merkel cell carcinoma cases, we investigated the expression of large T antigen *in vitro* and *in vivo*. Immunohistochemistry using a rabbit polyclonal antibody revealed that large T antigen was expressed in the nuclei of Merkel cell carcinoma cells with Merkel cell polyomavirus infection. Deletion mutant analyses identified an Arg–Lys–Arg–Lys sequence (amino acids 277–280) as a nuclear localization signal in large T antigen. Sequence analyses revealed that there were no mutations in the nuclear localization signal in any of the eleven Merkel cell polyomavirus strains examined. Furthermore, stop codons were not observed in the upstream of the nuclear localization signal in any of the Merkel cell carcinoma cases examined. These data suggest that the nuclear localization signal is highly conserved and functional in Merkel cell carcinoma cases.

Introduction

A newly identified polyomavirus, Merkel cell polyomavirus (MCPyV), was detected in Merkel cell carcinoma (MCC) in 2008 (Feng et al., 2008). The presence of MCPyV in MCC was confirmed in subsequent studies (Becker et al., 2009; Duncavage et al., 2009; Foulongne et al., 2008; Garneski et al., 2009; Kassem et al., 2008; Katano et al., 2009; Sastre-Garau et al., 2009). It was demonstrated that MCPyV becomes integrated into the host genome of tumor cells in some cases of MCC (Feng et al., 2008; Sastre-Garau et al., 2009). Similar to other polyomaviruses, the MCPyV genome encodes a large T (LT) antigen. The LT antigens of polyomaviruses are known to be potent oncoproteins that are capable of transforming various types of mammalian cells (DeCaprio, 2009; Levine, 2009; Pipas, 2009). MCPyV-LT antigen is thought to be a multifunctional protein, similar to SV40-LT antigen (Shuda et al., 2008). MCPyV-LT antigen consists of CR1, DnaJ, Rb-binding, origin-binding, zinc-binding domain, leucine zipper and helicase/ATPase domains. It has been demonstrated that SV40-LT antigen transforms mammalian cells and that SV40 infection induces tumorigenesis *in vivo* (Levine, 2009; Pipas, 2009). SV40-LT antigen binds to the tumor suppressor retinoblastoma protein (Rb) and inhibits its function, resulting in promotion of the cell cycle (DeCaprio, 2009). MCPyV-LT antigen has also been shown to have a functional Rb-binding site (Shuda et al., 2008), suggesting that it may play an important role in the oncogenesis of MCPyV. MCPyV-LT antigen also possesses a DNA helicase domain in its C-terminal region. The helicase activity of MCPyV-LT antigen is important for virus replication. However, MCPyV sequences derived from tumor cells of MCC have truncating mutations in the LT gene that result in defects of the C-terminal region of MCPyV-LT antigen in the tumors (Shuda et al., 2008). Loss of the C-terminal domain of MCPyV-LT impairs its helicase activity and virus replication ability. Consequently, the mutations in the MCPyV-LT gene promote its oncogenicity through its Rb-binding function, but do not allow viral DNA replication. Recently, an immunohistochemical study using an anti-MCPyV-LT mouse monoclonal antibody demonstrated expression of MCPyV-LT antigen in the nuclei of tumor cells from MCC cases with a high average PCR-quantified MCPyV genome level of 5.2 copies/cell of the LT gene (Shuda et al., 2009). This finding suggests that MCPyV infection is associated with the pathogenesis in a subset of MCC. The nuclear localization of MCPyV-LT antigen should be important for oncogenesis and DNA replication by MCPyV because MCPyV-LT antigen binds to Rb and expresses helicase activity in the nucleus. However, the nuclear localization signal (NLS) of MCPyV-LT antigen

* Corresponding author. Fax: +81 3 5285 1189.
E-mail address: katano@nih.go.jp (H. Katano).

0042-6822/$ – see front matter © 2009 Elsevier Inc. All rights reserved.
doi:10.1016/j.virol.2009.12.024

has not yet been identified. It also remains unknown whether the mutations in the MCPyV-LT gene alter the localization and functions of MCPyV-LT antigen. To clarify these issues, we established a polyclonal antibody against MCPyV-LT antigen, and detected the expression of LT antigen in MCC samples. In addition, we identified the NLS in MCPyV-LT antigen and investigated whether mutations around the NLS affect MCPyV-LT expression using deletion mutants and mutagenesis of MCPyV-LT antigen.

Results

MCPyV-LT expression in MCC cells

To investigate the expression of MCPyV-LT antigen in MCC samples, we established a rabbit polyclonal antibody against MCPyV-LT. Since the first exon of MCPyV-LT overlaps with small T antigen and the C-terminal region of MCPyV-LT is frequently truncated in MCC, a protein fragment comprising aa 79–334 encoded by nt 859–1628 was selected as the antigen for the anti-LT antibody (Shuda et al., 2009). A GST-MCPyV-LT (aa 79–334) fusion protein was used to immunize rabbits. Western blotting revealed that an affinity-purified rabbit polyclonal antibody against LT reacted with the GST-MCPyV-LT fusion protein in an *Escherichia coli* lysate, but not with GST protein alone (Fig. 1A). A previous report demonstrated that a full-length cDNA of the MCPyV-LT gene (3.0 kbp) produced several transcripts in transfectants, and that a 1.8-kb transcript (T4) was predominant (Shuda et al., 2008). Our western blotting analyses also revealed that the antibody reacted with 120-kDa and 57-kDa proteins in 293T cells transfected with pcDNA4HisMax-LT-wt (Fig. 1A). Immunohistochemical analyses revealed nuclear staining of the anti-MCPyV-LT polyclonal antibody in pcDNA4HisMax-LT-wt-transfected cells, but no staining in vector-transfected cells, indicating the specificity of the antibody (Fig. 1B). The immunohistochemical analyses further revealed that some, but not all, of the MCC cells expressed MCPyV-LT antigen in their nuclei (Fig. 1C and Table 1). The staining for MCPyV-LT antigen exhibited a diffuse and sometimes reticulated pattern in the nuclei of MCC cells. Although all of the 19 MCC cases examined were positive for cytokeratin 20, the expression of MCPyV-LT antigen differed among cases (Table 1). While 11 of the 19 MCC cases were positive for MCPyV by PCR, immunohistochemical analyses detected MCPyV-LT antigen in 7 of 10 MCPyV PCR-positive cases (70%). Based on the copy numbers of MCPyV, MCPyV-LT antigen was detected in cases with more than 0.05 MCPyV copies/cell (Table 1). In a few MCC cases, >80% of the MCC cells were positive for MCPyV-LT antigen, compared with <5% positivity or absence of staining in the other cases. No positive signals were detected in any of the MCPyV PCR-negative MCC cases. No nonspecific signals were observed in epithelial cells, blood vessels or lymphocytes in the skin, even in MCPyV-LT antigen-positive cases (Fig. 1C). In addition to the MCC samples, we examined the antibody staining in various organs such as lymph nodes, liver, spleen, brain, salivary glands, lung, pancreas, muscle, heart and uterus, but no specific signals were detected (data not shown). Moreover, 10 normal skin samples were negative for MCPyV-LT antigen. The antibody did not produce any signals in JCV-positive encephalitis and BKV-positive kidney samples, indicating a specific reaction with MCPyV-LT antigen (data not shown). These results demonstrate that MCPyV-LT antigen is expressed in the nuclei of MCC cells with >0.05 copies per cells of MCPyV.

MCPyV-LT antigen expression in transfectants

The *in vivo* expression findings for MCPyV-LT antigen in MCC cells suggested that nuclear localization is common among MCC cases. It

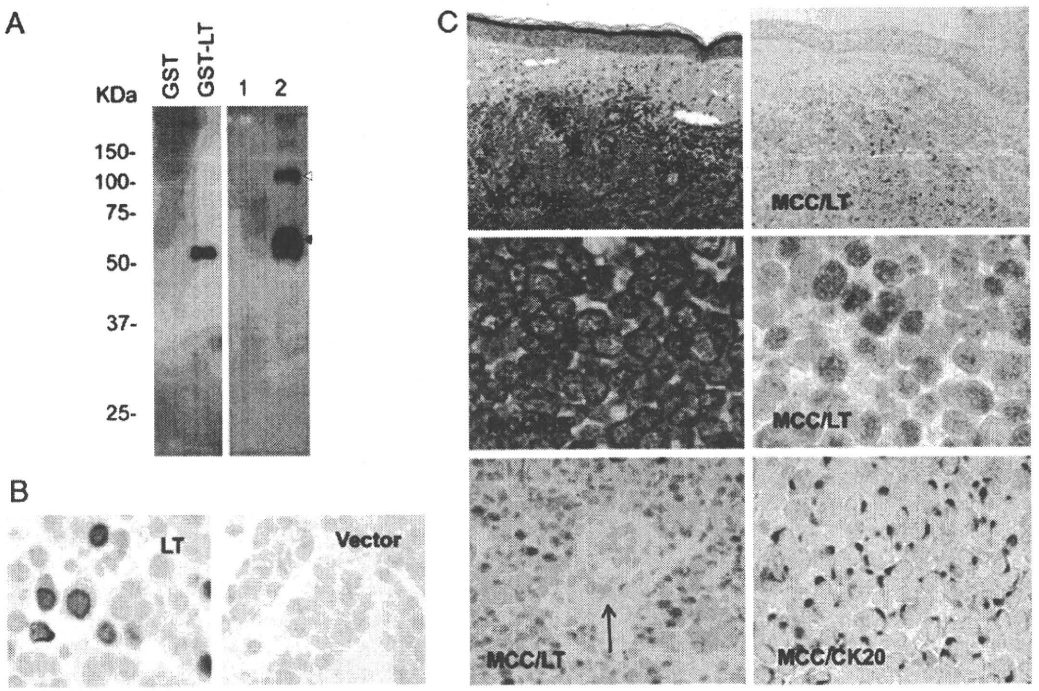

Fig. 1. Establishment of a polyclonal antibody against MCPyV-LT antigen and expression of MCPyV-LT antigen in MCC samples. (A) Western blotting. The affinity-purified rabbit polyclonal antibody reacts with GST-MCPyV-LT antigen (aa 79–334) and lysates of transfected 293T cells. 1: pcDNA4 HisMaxA vector; 2: pcDNA4HisMax-LT-wt. Open triangle: wild-type (full-length) MCPyV-LT antigen; closed triangle: 57kT wild-type antigen. (B) Immunohistochemistry of MCPyV-LT-transfected cells. The antibody stains the nuclei of pcDNA4HisMax-LT-wt-transfected 293T cells (left panel), but does not stain the nuclei of pcDNA4HisMax vector-transfected 293T cells (right panel). The nucleus was counterstained with hematoxylin. (C) Expression of MCPyV-LT antigen in MCC samples. Upper: low magnification views of an MCC sample. HE staining shows that MCC tumor cells have infiltrated the dermis of the skin (upper left). MCPyV-LT antigen is detected in tumor cells with the anti-MCPyV-LT antigen polyclonal antibody, but is not detected in epithelial cells and connecting tissue in the skin (upper right). Tumor cells are composed of round cells with bright nuclei (middle left). MCPyV-LT antigen is detected in the nuclei of tumor cells with a diffuse staining pattern (middle right). A blood vessel (arrow) is not stained by the antibody (lower left). Tumor cells are positive for cytokeratin 20 by immunohistochemistry (lower right).

Table 1
Relationships between the MCPyV copy numbers and LT expression. IHC: immunohistochemistry, ND: not done.

Sample	MCPyV-PCR	MCPyV copies/cell	MCPyV-LT -IHC	Cytokeratin 20
J1	+	11.943	+	+
J2	+	0.433	+	+
J3	+	0.206	+	+
J4	+	0.169	+	+
J5	+	0.119	ND	+
J6	+	0.073	+	+
J7	+	0.058	+	+
J8	+	0.056	+	+
J9	+	0.029	−	+
J10	+	0.018	+/−	+
J11	+	0.013	−	+
J12	−	0	−	+
J13	−	0	−	+
J14	−	0	−	+
J15	−	0	−	+
J16	−	0	−	+
J17	−	0	−	+
J18	−	0	−	+
J19	−	0	−	+

has also been demonstrated that SV40-LT antigen is localized in the nuclei of infected cells and transfectants (Jarvis et al., 1984; Kalderon et al., 1984). Transfection experiments using CV-1 cells revealed that RFP-tagged MCPyV-LT antigen was expressed in the nucleus with a diffuse staining pattern, whereas vector-transfected cells expressed RFP in the cytoplasm (Fig. 2A). Immunohistochemistry using anti-MCPyV-LT antibody demonstrated that MCPyV-LT antigen was expressed in the nucleus of pCXN2-mRFP-LT-wt- or pcDNA4His-Max-LT-wt-transfected 293T cells (Figs. 1B and 2B). These results indicate that MCPyV-LT antigen is localized in the nucleus not only *in vivo*, but also *in vitro*.

Identification of the NLS in the MCPyV-LT gene

The LT antigens of SV40, JCV and BKV have a conserved amino acid NLS motif, KKKR(or K)KVEDP and other two human polyomaviruses KI and WU have similar motifs (Fig. 3) (Kalderon et al., 1984). However, MCPyV-LT antigen does not contain such a motif at analogous positions. The PredictNLS, an online prediction system for NLS sequences (http://www.predictprotein.org/cgi/var/nair/resonline.pl), suggested a sequence of amino acids (aa 277–304

Fig. 3. Alignment of amino acid sequences around NLS among human polyomaviruses by Clustal W. A conserved amino acid NLS motif in SV40, JCV, and BKV is indicated by a bold black bar. A bold break line indicates a putative NLS of MCPyV-LT antigen suggested by the PredictNLS, an online prediction system for NLS sequences.

encoded by nt 1455–1538) as an NLS. To identify the NLS in MCPyV-LT antigen, deletion mutants of the MCPyV-LT gene were constructed in a plasmid and expressed as fusion proteins with RFP (Fig. 4A). The LTdel-2 and -4 proteins showed nuclear localization, whereas the LTdel-1, -3 and -5 proteins did not, suggesting that the NLS existed within aa 211–332 (Figs. 4A–C). Moreover, transfection into CV-1 cells revealed that LT1–280 and LT1–304 were localized in the nucleus, but LT1–276 was localized in the cytoplasm, suggesting the presence of the NLS within aa 277–280 (RKRK, Figs. 4A and C, data not shown). Mutagenesis analyses showed that an amino acid change of lysine at position 278 to threonine in the full-length MCPyV-LT antigen impaired the nuclear localization of MCPyV-LT antigen (Fig. 4C). Western blotting confirmed that all the constructs produced RFP fusion proteins with predicted sizes in the transfected cells (Fig. 4B). Transfection also demonstrated nuclear localization of GFP-RKRK or GFP-RKRT fusion protein, but cytoplasmic localization of GFP or GFP-RTRK fusion protein in transfectants (Fig. 4D). These data clearly showed that the NLS was aa 277–280 (RKRK; Arg–Lys–Arg–Lys; nt 1455–1466) in MCPyV-LT antigen and that Lys-278 is a responsible amino acid for the nuclear localization of MCPyV-LT antigen.

Mutations in the NLS in cases of MCC

Since mutations are frequently detected in the MCPyV-LT gene (Shuda et al., 2008), we investigated whether such mutations alter the

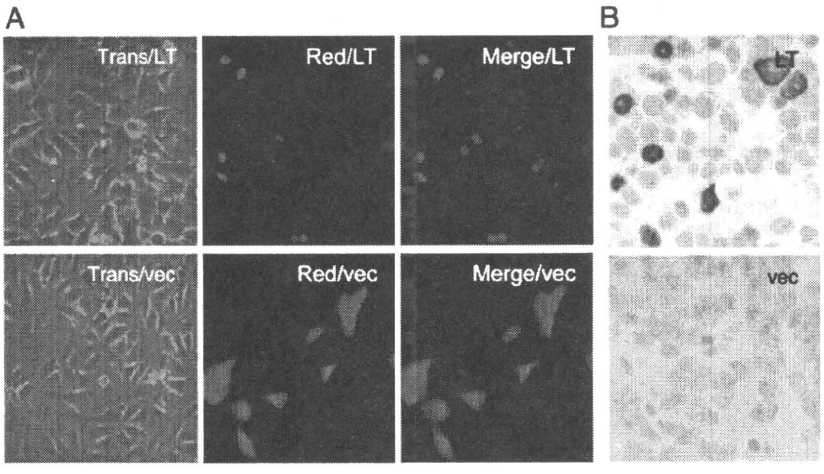

Fig. 2. Nuclear localization of MCPyV-LT antigen in transfected cells. (A) Fluorescence images of RFP-tagged MCPyV-LT antigen in transfected CV-1 cells. RFP-tagged MCPyV-LT antigen is expressed in the nuclei of the transfected cells (upper panels), whereas vector-transfected cells express RFP in the cytoplasm (lower panels). (B) Immunohistochemistry using anti-MCPyV-LT antibody of RFP-tagged MCPyV-LT antigen in transfected 293T cells. MCPyV-LT antigen was detected in the nucleus of pCXN2-mRFP-LT-wt-transfected 293T cells (upper panel), but not in vector-transfected cells (lower panel). The nucleus was counterstained with hematoxylin.

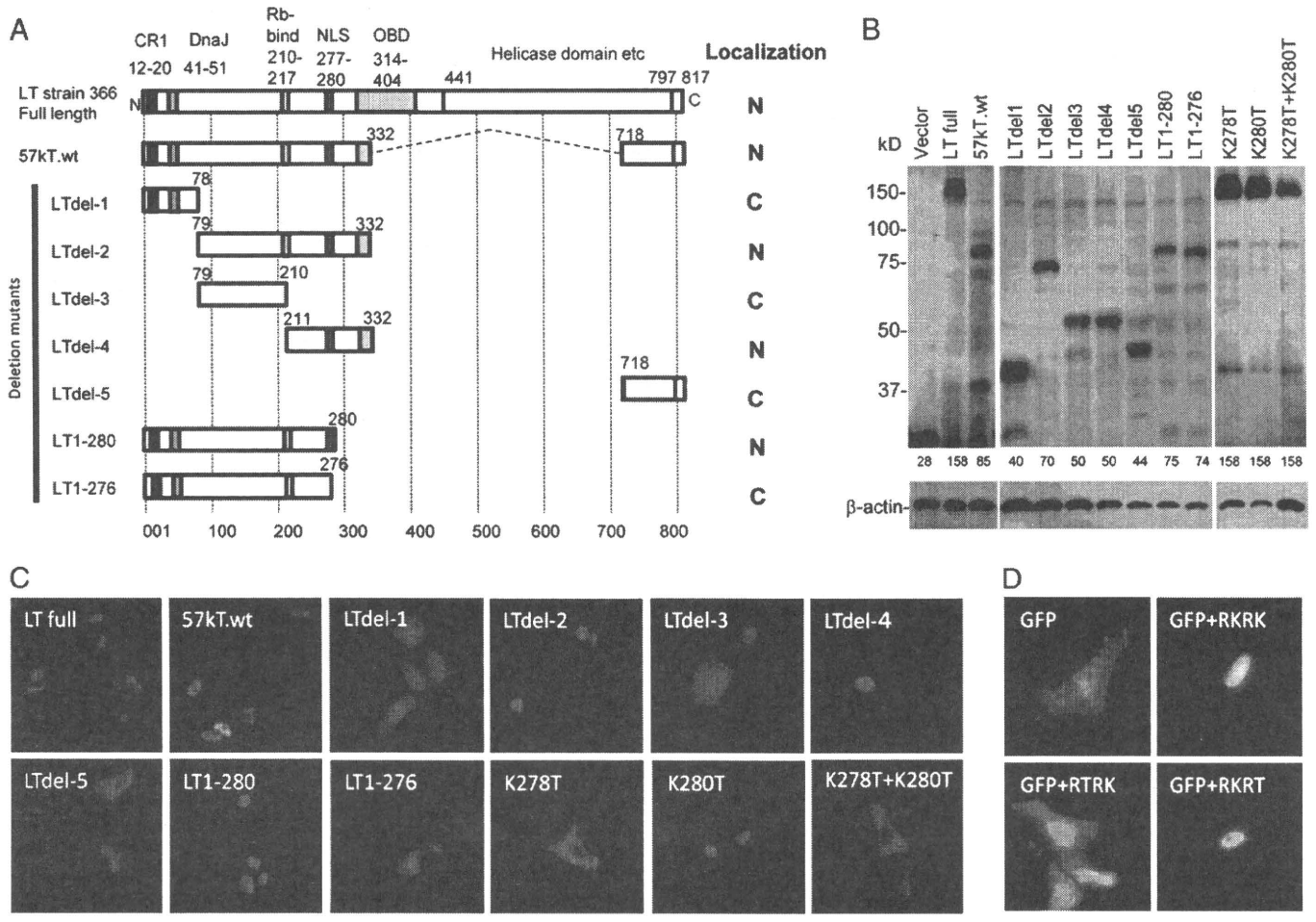

Fig. 4. Determination of the NLS in MCPyV-LT antigen. (A) Deletion mutants of MCPyV-LT. Seven fragments of the MCPyV-LT gene were cloned into the pCXN2-mRFP vector (LTdel-1, -2, -3, -4, -5, LT1–276 and LT1–280). The putative NLS is shown as a red box. The numbers indicate the amino acid positions in MCPyV-LT antigen of MCC 366 strain (GenBank ACl25294). The localizations on the right indicate the nuclear (N) and cytoplasmic (C) localizations of the mutants in transfected cells. (B) Western blotting analysis of deletion mutants and mutagenesis. Each plasmid expressed a mutant or mutagenesis with a predicted size. The predicted sizes are shown at the bottom of the upper panel. K278T and K280T indicate mutagenesis of K to T at aa 278 and aa 280 in the wild-type MCPyV-LT antigen, respectively. K278T+K280T indicates a dual mutant of aa 278 and aa 280. (C) RFP expression in cells transfected with the deletion mutants. (D) EGFP expression in cells transfected with pEGFP vector (upper left), pEGFP-RKRK (upper right), pEGFP-RTRK (lower left) and pEGFP-RKRT (lower right).

expression of MCPyV-LT antigen *in vivo*. A previous report showed that all first stop codons detected to date were located between nt 1401 and nt 2234 in the MCPyV-LT gene (Shuda et al., 2008). The NLS was located at nt 1455–1466. Therefore, we carried out PCR to amplify a DNA fragment from nt 1361 to 1503 containing the NLS in 9 Japanese cases of MCC and 2 cases of Kaposi's sarcoma with MCPyV infection (Katano et al., 2009). The DNA sequences of these PCR products revealed that mutations with stop codons were detected in the downstream of the NLS in 5 of the 11 cases (Fig. 5A). However, no mutations with stop codons were detected in the upstream of the NLS in any of the cases examined (Fig. 5A). Although mutations with amino acid changes were frequently detected around the NLS, there were no mutations in the NLS region of the MCPyV-LT gene, indicating that the NLS was highly conserved (Fig. 5B). These data suggest that the NLS of MCPyV-LT antigen is functional in clinical samples.

Discussion

In the present study, we have demonstrated the nuclear localization of MCPyV-LT antigen *in vitro* and in cases of MCC. The NLS was located between the Rb-binding and DNA helicase domains. Mutations with stop codons were not detected in the upstream of the NLS, and the NLS sequence was highly conserved in the MCC samples.

Nuclear expression of MCPyV-LT antigen in MCC has already been demonstrated in a recent report (Shuda et al., 2009). In that study, a monoclonal antibody against a short peptide of MCPyV-LT antigen was established, and showed diffuse signals in the nuclei of MCC tumor cells (Shuda et al., 2009). Since our polyclonal antibody targeted a middle region of MCPyV-LT antigen comprising a 252-aa protein, its reactivity should be broader than that of the monoclonal antibody established against a peptide. Moreover, a recent serological study revealed that infection with an African green monkey B-lymphotropic polyomavirus-like virus was common among humans (Kean et al. 2009), suggesting that the polyclonal antibody could theoretically detect the T antigens of known or undiscovered nearer relatives of MCPyV. However, the positive signals for MCPyV-LT antigen were limited and partial in the MCC samples examined. The results of our immunohistochemical analyses using the anti-MCPyV-LT polyclonal antibody correlated well with those of MCPyV-PCR and real-time PCR (Table 1), suggesting the specificity of the polyclonal antibody to MCPyV-LT antigen. Our antibody detected MCPyV-LT antigen in cases with >0.05 copies/cell of the LT gene, whereas the previous study detected MCPyV-LT antigen expression in cases with 0.8–14 copies/cell (Shuda et al., 2009). Since all the MCC samples investigated in the present study were paraffin-embedded samples, it was impossible to detect MCPyV by Southern blot hybridization. However, the anti-MCPyV-LT polyclonal antibody was able to detect MCPyV-LT antigen in

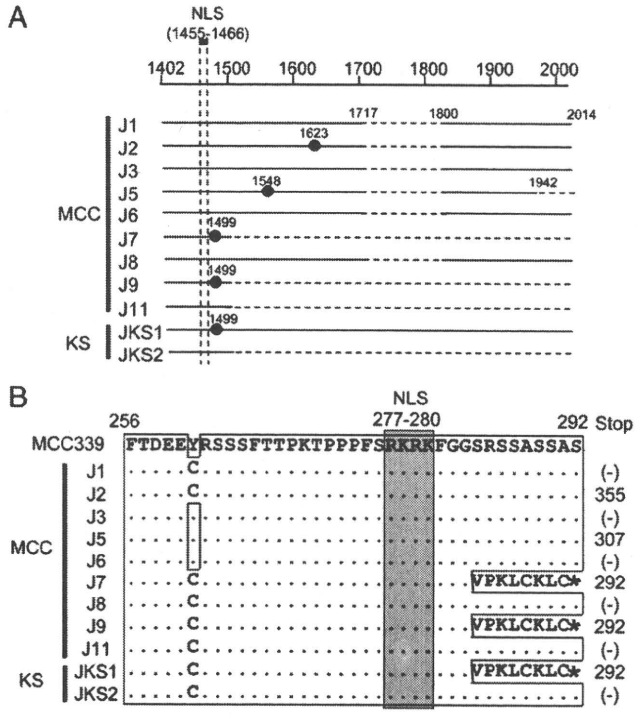

Fig. 5. The NLS and mutations of the MCPyV-LT gene. (A) Locations of the first stop codons in 9 samples of MCC and 2 samples of Kaposi's sarcoma (KS). The NLS is shown as a vertical box with a broken line. The first stop codon is shown as a closed circle in each strain. The first stop codons are located on the C-terminal side of the NLS. The solid lines indicate sequenced fragments, while the dashed lines indicate unsequenced regions. (B) Amino acid sequences around the NLS. Amino acid changes are indicated by outlined characters, and stop codons are indicated by asterisks. The positions of the first stop codons are listed on the right. (—) indicates that no stop codon was detected.

cases with relatively low copy numbers of MCPyV (Table 1). Overall, 7 of 10 (70%) MCPyV-positive MCC samples were positive for MCPyV-LT antigen by immunohistochemistry, representing a similar rate to that reported by Shuda et al. (2009). These findings support the idea that MCPyV is associated with the pathogenesis in some, but not all, MCC cases. In addition, our immunohistochemical analyses showed that the expression of MCPyV-LT antigen even differed among cells within MCPyV-positive MCC cases. MCPyV-LT antigen is a putative oncogenic protein encoded by MCPyV, but its transformation activity has not yet been demonstrated. Further studies are required to clarify the expression and oncogenic function of MCPyV-LT antigen. Our anti-MCPyV-LT antibody is a useful tool for detecting MCPyV infection, but it is to be noted for a diagnosis of MCC that a subset of MCC are negative for MCPyV.

Sun exposure of the skin may induce DNA mutations in the MCPyV genome, and the MCPyV-LT gene may be a frequent target for mutations. Our findings of mutations in the MCPyV-LT gene around the NLS suggest a relationship between mutations and the functions of MCPyV-LT antigen. All mutations with a first stop codon identified to date have been detected between nt 1401 (MCC350 strain; GenBank EU375803) and nt 2234 (MCC339 strain; GenBank EU375804). If there are no stop codon mutations in the MCPyV-LT gene, MCPyV-LT antigen induces viral replication using its DNA helicase domain (Shuda et al., 2008). If a mutation with a stop codon is inserted into the downstream (nt 1467–2234) of the NLS, the truncated MCPyV-LT antigen induces oncogenesis through its Rb-binding domain without DNA replication. If a mutation with a stop codon is inserted into the upstream (nt 1401–1454) of the NLS, the truncated MCPyV-LT antigen without the NLS is unable to express itself in the nucleus. Then, how does the truncated MCPyV-LT antigen without the NLS contribute to tumor formation? Although our MCC samples had no mutations with stop codons in the upstream of the NLS, two sequences of MCPyV reported previously had a mutation with a stop codon before the NLS (Shuda et al., 2008). These strains are both American strains, MCC350 and MCC344, and have mutations with stop codons at nt 1401 and nt 1452, respectively. These mutations result in stop codons at aa 259 and aa 276, just upstream of the NLS (aa 277–280). These two cases suggest that NLS-truncating mutations are uncommon in MCC, and the truncated MCPyV-LT antigen without the NLS can nevertheless be associated with MCC tumor formation.

In conclusion, we have demonstrated MCPyV-LT antigen expression in MCC cells and identified the NLS in the MCPyV-LT gene. Sequence analyses of clinical samples suggested that mutations around the NLS alter the functions of MCPyV-LT antigen. Sun exposure is thought to be a crucial factor in the pathogenesis of MCC, and the present findings suggest that mutations caused by sun exposure are associated with MCPyV pathogenesis.

Materials and methods

Synthesis and purification of recombinant GST-MCPyV-LT

A DNA fragment corresponding to nucleotides (nt) 859–1628 of the MCPyV gene (GenBank accession number EU375803) was PCR-amplified from a DNA sample extracted from a case of MCPyV-positive Kaposi's sarcoma (Katano et al., 2009). The forward primer sequence was 5′-CTGgaattcAGGTTGACGAGGCCCCTATAT-3′ and the reverse primer sequence was 5′-GCGctcgagATTTGCTGTTTTATTACTATA-3′ (the cloning sites are shown in lowercase letters). After purification by agarose gel electrophoresis, the PCR product was cloned into the *Eco*RI/*Xho*I sites of the bacterial expression vector pGEX5X-2 (GE Healthcare BioSciences, Piscataway, NJ). The resulting expression vector produced 256 amino acids of MCPyV-LT as a fusion protein with glutathione-S transferase (GST) in *Escherichia coli* (JM109; Toyobo, Toyama, Japan). The fusion protein (GST-MCPyV-LT) was affinity-purified using glutathione-Sepharose as described previously (Smith and Johnson, 1988). The purity and concentration of the eluted protein were assessed by sodium dodecyl sulfate-polyacrylamide gel electrophoresis and the Bradford assay (Protein Assay; Bio-Rad, New York, NY), respectively.

Production of an anti-MCPyV-LT antibody

Purified GST-MCPyV-LT fusion protein was used by MBL (Medical & Biological Laboratories, Nagoya, Japan) to immunize New Zealand white rabbits for the production of anti-MCPyV-LT polyclonal antibodies. Immune sera collected from the rabbits were partially purified twice by ammonium sulfate precipitation and the precipitates were dissolved in PBS. The protein solution was passed through a GST-Sepharose column to remove anti-GST antibodies before the desired antibody was affinity-purified using GST-MCPyV-LT coupled to activated CH-Sepharose (GE Healthcare BioSciences). The purified antibody was used in the subsequent experiments.

Plasmids and transfection

To construct pcDNA4HisMax-LT-wt, a 3.0-kbp full-length cDNA of the wild-type LT gene was PCR-amplified from a DNA sample extracted from a case of MCPyV-positive Kaposi's sarcoma using forward (5′-CACggtaccGGATTTAGTCCTAAATAGGAA-3′) and reverse (5′-CACctcgagTTGAGAAAAAGTACCAGAATC-3′) primers (Katano et al., 2009). The PCR product was cloned into the *Kpn*I/*Xho*I sites of pcDNA4HisMaxA (Invitrogen, Carlsbad, CA) to create pcDNA4HisMax-LT-wt. To construct pCXN2-mRFP-LT-wt, the LT gene was PCR-amplified from pcDNA4HisMax-LT-wt using forward (Merkel LT-*Xho*I-F, 5′-CGCctcgagATGGATTTAGTCCTAAATAGG-3′) and reverse

(Merkel LT-*Not*I-R, 5′-ATATAgcggccgcTTATTGAGAAAAAGTACCA-3′) primers. The PCR product was cloned into the *Xho*I/*Not*I sites of pCXN2-mRFP (a kind gift from Dr. Michiyuki Matsuda, Kyoto University, Kyoto, Japan) (Niwa et al., 1991). To construct pCXN2-mRFP-LT-57kTwt, a 1.8-kb LT transcript (T4) was amplified by RT-PCR from RNA extracted from pcDNA4HisMax-LT-wt-transfected 293T cells using the Merkel LT-*Xho*I-F and Merkel LT-*Not*I-R primers (Shuda et al., 2008). Expression plasmids were transfected into CV-1 or 293T cells using Fugene 6 (Roche Diagnostics, Indianapolis, IN) according to the manufacturer's instructions.

Western blotting

Cell extract preparation and immunoblotting analyses were performed as described previously (Katano et al., 2001). Proteins were separated by sodium dodecyl sulfate-polyacrylamide gel electrophoresis, electrotransferred to membranes and probed with the rabbit anti-MCPyV-LT polyclonal antibody (diluted 1:10,000) or a rabbit anti-red fluorescent protein (RFP) antibody (diluted 1:5,000; BD Biosciences Clontech, Mountain View, CA). The membranes were then incubated with a horseradish peroxidase-conjugated anti-rabbit secondary antibody (BioSource International, Camarillo, CA) and visualized with Super Signal Westdura (Thermo Fisher Scientific, Waltham, MA). For signal amplification, a Can Get Signal amplification kit (Toyobo, Osaka, Japan) was used according to the manufacturer's instructions. As an internal control protein, β-actin was detected with an anti-β-actin antibody (Sigma-Aldrich, St. Louis, MO) after stripping the membranes.

Clinical samples

Studies using human tissues were performed with the approval of the Institutional Review Board of the National Institute of Infectious Diseases (Approval No. 192). Nineteen formalin-fixed paraffin-embedded tissue samples of MCC were collected. Among them, 11 cases were positive for MCPyV by PCR (Table 1). In addition, anonymous archival samples of various organs were used for immunohistochemical analyses.

Real-time PCR

The copy numbers of MCPyV-LT DNA were determined by quantitative real-time TaqMan PCR using an Mx3005P real-time PCR system (Stratagene, La Jolla, CA). The amount of human genomic DNA (β-actin gene) present in the DNA extracted from each specimen was also determined. To amplify MCPyV-LT, forward (Merkel PV LT Forward: 5′-TCTGGGTATGGGTCCTTCTCA-3′) and reverse (Merkel PV LT Reverse: 5′-TGGTGTTCGGGAGGTATATCG-3′) primers were used with the labeled probe 5′-(FAM)CGTCCCAGGCTTCAGACTCCCAGTC (TAMRA)-3′ (Katano et al., 2009). To amplify β-actin DNA, forward (5′-TGAGCGCGGCTACAGCTT-3′) and reverse (5′-TCCTTAATGTCACG-CACGATTT-3′) primers were used with the labeled probe 5′-(FAM) ACCACCACGGCCGAGCGG(TAMRA)-3′ (Kuramochi et al., 2006). The amplicon sizes of MCPyV-LT and β-actin were 77 bp (nt 1053–1129 in GenBank EU375803) and 60 bp (nt 655–714 in NM_001101), respectively. PCR amplification was performed in 20-μL reaction mixtures using QuantiTect probe PCR Master Mix (Qiagen GmbH, Hilden, Germany), 0.3 μM of each primer, 0.3 μM of TaqMan probe and 2 μL of isolated DNA. The PCR conditions were 95 °C for 15 min, followed by 40 cycles of 94 °C for 15 s and 60 °C for 1 min. Quantitative results were obtained by generating standard curves for pCR2.1 plasmids (Invitrogen) containing each MCPyV-LT and cellular target (β-actin gene) amplicon. Virus copy numbers/cell were calculated by dividing the MCPyV-LT copy numbers by half of the β-actin copy numbers, because each cell contains two copies of DNA in two alleles (Asahi-Ozaki et al., 2006).

Immunohistochemistry

Formalin-fixed MCC specimens were embedded in paraffin, sectioned and stained with hematoxylin and eosin (HE). Immunohistochemistry was performed with the rabbit anti-MCPyV-LT polyclonal antibody as the primary antibody. As the second and third phase reagents for immunostaining, a biotinylated F(ab')2 fragment of goat anti-rabbit immunoglobulin (Dako, Copenhagen, Denmark) and peroxidase-conjugated streptavidin (Dako) were used, respectively. The secondary antibody signals were amplified with a catalyzed signal amplification kit II (Dako). The details of the immunostaining procedure were described previously (Katano et al., 1999).

Alignment of LT sequences

LT sequences of SV40, JCV, BKV, WU, KI and MCPyV were obtained from the GenBank database (accession numbers: NP_043127, NP_043512, YP_717940, ACB12032, ABR68683 and ACI25312) and aligned using ClustalW.

Deletion mutants and mutagenesis

Seven fragments of the LT gene were amplified using the following primers: Merkel LT-*Xho*I-F and Merkel LT-*Not*I-426R (5′-ATA-TAgcggccgcTTAATCAAACATAGAGAAGT-3′) for LTdel-1 (amino acids (aa) 1–78 in GenBank ACI25294); Merkel LT-*Xho*I-861F (5′-CGCctcgagGTTGACGAGGCCCCTATATAT-3′) and Merkel LT-*Not*I-1622R (5′-ATATAgcggccgcTTATGTTTTATTACTATATA-3′) for LTdel-2 (aa 79–332); Merkel LT-*Xho*I-861F and Merkel LT-*Not*I-1256R (5′-ATATAgcggccgcTTACTCCCAGGTGCCATCCG-3′) for LTdel-3 (aa 79–210); Merkel LT-*Xho*I-1257F (5′-CGCctcgagGATCTCTTCTGCGAT-GAATCA-3′) and Merkel LT-*Not*I-1622R for LTdel-4 (aa 211–332); Merkel LT-*Xho*I-2778F (5′-CGCctcgagGCAAATCTAAGAGATTCCCTG-3′) and Merkel LT-*Not*I-R for LTdel-5 (aa 718–817); Merkel LT-*Xho*I-F and Merkel LT-*Not*I-1539R (5′-ATATAgcggccgcTTATTTTTTGGCTTTGGTG-GAG-3′) for LT1-280 (aa 1–280); and Merkel LT-*Xho*I-F and Merkel LT-*Not*I-1456R (5′-ATATAgcggccgcTTATTCTTGAGAATGGAGGA-3′) for LT1-276 (aa 1–276). All the gene fragments were amplified from pcDNA4HisMax-LT-wt and subcloned into the *Xho*I/*Not*I sites of the pCXN2-mRFP vector. Mutagenesis was performed on pCXN2-mRFP-LT-wt using a QuickChange Site-directed Mutagenesis kit (Stratagene). To construct pEGFP-RKRK, pEGFP-RTRK, and pEGFP-RKRT, following oligomers were hybridized, and digested with *Xho*I/*Bam*HI: 5′-AACCTCGAGAGAAAGCGAAAAGGATCCAAC-3′ and 5′-GTTGGATCCTTTTCGCTTTCTCTCGAGGTT-3′ for pEGFP-RKRK, 5′-AACCTCGAGAGAACGCGAAAAGGATCCAAC-3′ and 5′-GTTGGATCCTTTTCGCGTTCTCTCGAGGTT-3′ for pEGFP-RTRK, and 5′-AACCTCGAGAGAAAGCGAACAGGATCCAAC-3′ and 5′-GTTGGATCCTGTTCGCTTTCTCTCGAGGTT-3′ for pEGFP-RKRT. Digested fragments were purified with PCR purification kit (Qiagen), and cloned into *Xho*I/*Bam*HI sites of the pEGFP-C3 (Clontech). Insertion of the NLS sequences in the pEGFP-C3 was confirmed with DNA sequencing.

DNA sequences

Fragments of LT (nt 1252–2013) were PCR-amplified using the following primers: MCPyV-LT 1250F (5′-GGGAGGATCTCTTCTGCGAT-3′) and MCPyV-LT 1382R (5′-GACGAGGCCTCCTCGGCAGA-3′) for nt 1252–1384; MCPyV-LT 1480F (5′-AAGCTCTGCAAGCTCTGCTA-3′) and MCPyV-LT 1605R (5′-ACAGCATGGCTAAGATAATC-3′) for nt 1481–1606; MCPyV-LT 1583F (5′-TCTGATTATCTTAGCCATGC-3′) and MCPyV-LT 1716R (5′-GCATGCCTGCTTTTAAAATC-3′) for nt 1584–1717; MCPyV-LT 1799F (5′-TGCACTATAAGCTTTTTAAT-3′) and MCPyV-LT 1941R (5′-CTGGCCTCTTTTTCTTTTTC-3′) for nt 1800–1942; and MCPyV-LT 1870F (5′-CCCTTACAAATTACTGCAAG-3′) and

MCPyV-LT 2012R (5′-GGGCTAAGATAATAAAGTGG-3′) for nt 1871–2013. To amplify the fragment for nt 1361–1503, nested PCR was performed using MCPyV-LT 1331F (5′-CAAGAAGCTCGCCCCGGCAG-3′) and MCPyV-LT 1522R (5′-AGTGCTTGTAAAACTTGCTG-3′) as the outer primers, and MCPyV-LT 1359F (5′-TTCCTCTGCCGAGGAGGCCT-3′) and MCPyV-LT 1522R as the inner primers. The PCR products were directly sequenced with an ABI Prism 3130 Genetic Analyzer (Applied Biosystems, Foster City, CA) using the PCR primers. The sequences were registered in the Genbank as accession numbers GQ888633 (J1), GQ888634 (J2), GQ888635 (J3), GQ888636 (J5), GQ888637 (J6), GQ888638 (J7), GQ888639 (J8), GQ888640 (J9), GQ888641 (J11), FJ464337 (JKS1), and GQ888642 (JKS2).

Acknowledgments

We thank Drs. Akira Suzuki and Yuichiro Fukasawa, Department of Clinical Laboratory, KKR Sapporo Medical Center, Toshihiko Iizuka and Hisako Endo, Department of Pathology, International Medical Center of Japan, for providing clinical samples. This work was partly supported by a Grant-in-Aid for Scientific Research C-21590520 (to HK) from the Ministry of Education, Culture, Sports, Science and Technology of Japan, Health and Labor Sciences Research Grants (H21-AIDS-Ippan-006 to HK, H20-Nanchi-Ippan-035 to TS, H20-Shinko-Ippan-006 to TS, H21-Shinko-Ippan-009 to HK) from the Ministry of Health, Labor and Welfare, and a grant for Research on Publicly Essential Drugs and Medical Devices SAA4832 (to HK and TS) from the Japan Health Sciences Foundation.

References

Asahi-Ozaki, Y., Sato, Y., Kanno, T., Sata, T., Katano, H., 2006. Quantitative analysis of Kaposi sarcoma-associated herpesvirus (KSHV) in KSHV-associated diseases. J. Infect. Dis. 193, 773–782.

Becker, J.C., Houben, R., Ugurel, S., Trefzer, U., Pfohler, C., Schrama, D., 2009. MC polyomavirus is frequently present in Merkel cell carcinoma of European patients. J. Invest. Dermatol. 129, 248–250.

DeCaprio, J.A., 2009. How the Rb tumor suppressor structure and function was revealed by the study of Adenovirus and SV40. Virology 384, 274–284.

Duncavage, E.J., Zehnbauer, B.A., Pfeifer, J.D., 2009. Prevalence of Merkel cell polyomavirus in Merkel cell carcinoma. Mod. Pathol. 22, 516–521.

Feng, H., Shuda, M., Chang, Y., Moore, P.S., 2008. Clonal integration of a polyomavirus in human Merkel cell carcinoma. Science 319, 1096–1100.

Foulongne, V., Kluger, N., Dereure, O., Brieu, N., Guillot, B., Segondy, M., 2008. Merkel cell polyomavirus and Merkel cell carcinoma, France. Emerg. Infect. Dis. 14, 1491–1493.

Garneski, K.M., Warcola, A.H., Feng, Q., Kiviat, N.B., Leonard, J.H., Nghiem, P., 2009. Merkel cell polyomavirus is more frequently present in North American than Australian Merkel cell carcinoma tumors. J. Invest. Dermatol. 129, 246–248.

Jarvis, D.L., Lanford, R.E., Butel, J.S., 1984. Structural comparisons of wild-type and nuclear transport-defective simian virus 40 large tumor antigens. Virology 134, 168–176.

Kalderon, D., Roberts, B.L., Richardson, W.D., Smith, A.E., 1984. A short amino acid sequence able to specify nuclear location. Cell 39, 499–509.

Kassem, A., Schopflin, A., Diaz, C., Weyers, W., Stickeler, E., Werner, M., Zur Hausen, A., 2008. Frequent detection of Merkel cell polyomavirus in human Merkel cell carcinomas and identification of a unique deletion in the VP1 gene. Cancer Res. 68, 5009–5013.

Katano, H., Sato, Y., Kurata, T., Mori, S., Sata, T., 1999. High expression of HHV-8-encoded ORF73 protein in spindle-shaped cells of Kaposi's sarcoma. Am. J. Pathol. 155, 47–52.

Katano, H., Ogawa-Goto, K., Hasegawa, H., Kurata, T., Sata, T., 2001. Human-herpesvirus-8-encoded K8 protein colocalizes with the promyelocytic leukemia protein (PML) bodies and recruits p53 to the PML bodies. Virology 286, 446–455.

Katano, H., Ito, H., Suzuki, Y., Nakamura, T., Sato, Y., Tsuji, T., Matsuo, K., Nakagawa, H., Sata, T., 2009. Detection of Merkel cell polyomavirus in Merkel cell carcinoma and Kaposi's sarcoma. J. Med. Virol. 81, 1951–1958.

Kean, J.M., Rao, S., Wang, M., Garcea, R.L., 2009. Seroepidemiology of human polyomaviruses. PLoS Pathog. 5, e1000363.

Kuramochi, H., Hayashi, K., Uchida, K., Miyakura, S., Shimizu, D., Vallbohmer, D., Park, S., Danenberg, K.D., Takasaki, K., Danenberg, P.V., 2006. Vascular endothelial growth factor messenger RNA expression level is preserved in liver metastases compared with corresponding primary colorectal cancer. Clin. Cancer Res. 12, 29–33.

Levine, A.J., 2009. The common mechanisms of transformation by the small DNA tumor viruses: the inactivation of tumor suppressor gene products: p53. Virology 384, 285–293.

Niwa, H., Yamamura, K., Miyazaki, J., 1991. Efficient selection for high-expression transfectants with a novel eukaryotic vector. Gene 108, 193–199.

Pipas, J.M., 2009. SV40: cell transformation and tumorigenesis. Virology 384, 294–303.

Sastre-Garau, X., Peter, M., Avril, M.F., Laude, H., Couturier, J., Rozenberg, F., Almeida, A., Boitier, F., Carlotti, A., Couturaud, B., Dupin, N., 2009. Merkel cell carcinoma of the skin: pathological and molecular evidence for a causative role of MCV in oncogenesis. J. Pathol. 218, 48–56.

Shuda, M., Feng, H., Kwun, H.J., Rosen, S.T., Gjoerup, O., Moore, P.S., Chang, Y., 2008. T antigen mutations are a human tumor-specific signature for Merkel cell polyomavirus. Proc. Natl. Acad. Sci. U.S.A. 105, 16272–16277.

Shuda, M., Arora, R., Kwun, H.J., Feng, H., Sarid, R., Fernandez-Figueras, M.T., Tolstov, Y., Gjoerup, O., Mansukhani, M.M., Swerdlow, S.H., Chaudhary, P.M., Kirkwood, J.M., Nalesnik, M.A., Kant, J.A., Weiss, L.M., Moore, P.S., Chang, Y., 2009. Human Merkel cell polyomavirus infection I. MCV T antigen expression in Merkel cell carcinoma, lymphoid tissues and lymphoid tumors. Int. J. Cancer Electronic Publication.

Smith, D.B., Johnson, K.S., 1988. Single-step purification of polypeptides expressed in Escherichia coli as fusions with glutathione S-transferase. Gene 67, 31–40.

Journal of Medical Virology 83:322–330 (2011)

A Novel Real-Time PCR System for Simultaneous Detection of Human Viruses in Clinical Samples From Patients With Uncertain Diagnoses

Harutaka Katano,[1]* Motofumi Kano,[1] Tomoyuki Nakamura,[1] Takayuki Kanno,[1] Hideki Asanuma,[2] and Tetsutaro Sata[1]

[1]*Department of Pathology, National Institute of Infectious Diseases, Shinjuku, Tokyo, Japan*
[2]*Influenza Virus Research Center, National Institute of Infectious Diseases, Shinjuku, Tokyo, Japan*

A novel simultaneous detection system for human viruses was developed using a real-time polymerase chain reaction (PCR) system to identify causes of infection in clinical samples from patients with uncertain diagnoses. This system, designated as the "multivirus real-time PCR," has the potential to detect 163 human viruses (47 DNA viruses and 116 RNA viruses) in a 96-well plate simultaneously. The specificity and sensitivity of each probe–primer set were confirmed with cells or tissues infected with specific viruses. The multivirus real-time PCR system showed profiles of virus infection in 20 autopsies of acquired immunodeficiency syndrome patients, and detected frequently TT virus, cytomegalovirus, human herpesvirus 6, and Epstein–Barr virus in various organs; however, RNA viruses were detected rarely except for human immunodeficiency virus-1. Pathology samples from 40 patients with uncertain diagnoses were examined, including cases of encephalitis, hepatitis, and myocarditis. Herpes simplex virus 1, human herpesvirus 6, and parechovirus 3 were identified as causes of diseases in four cases of encephalitis, while no viruses were identified in other cases as causing disease. This multivirus real-time PCR system can be useful for detecting virus in specimens from patients with uncertain diagnoses. ***J. Med. Virol. 83:322–330, 2011.***

KEY WORDS: real-time PCR; acquired immunodeficiency syndrome (AIDS); virus; autopsy

INTRODUCTION

Polymerase chain reaction (PCR) is a powerful tool to detect viruses compared with some traditional methods such as the direct fluorescent-antibody assay or virus isolation in cell culture. Real-time PCR is a sensitive system to detect viral genomes, used commonly worldwide [Storch, 2000]. Moreover, multiplex PCR fluorescence techniques are able to identify several genes in one tube simultaneously. Some reports have described simultaneous detection systems for up to 20 viruses using real-time PCR or conventional PCR [Vet et al., 1999; Bellau-Pujol et al., 2005; Li et al., 2007; Mahony et al., 2007; Molenkamp et al., 2007; Nolte et al., 2007; van de Pol et al., 2007; Wada et al., 2009]. However, the number of viruses detectable in one tube is limited by fluorescence wavelength. On the other hand, microarray analysis can detect a large number of viruses simultaneously. The weak point of the microarray assay is its low sensitivity and specificity [Wang et al., 2002].

It has been demonstrated that many viruses are associated with human diseases, and such human pathogenic viruses include both DNA and RNA viruses. An ideal virus screening system may be a system capable of detecting all the human pathogenic viruses simultaneously. In the present study, a real-time PCR system capable of detecting more than one hundred human viruses in a 96-well reaction plate simultaneously was established, designated as the "multivirus real-time PCR" system. In this system, two viruses are detected in one well using a duplex TaqMan real-time reverse transcriptase (RT)-PCR system; since more than 82 different duplex real-time PCRs are performed in a 96-well plate except wells for standard curve and

Additional Supporting Information may be found in the online version of this article.

Grant sponsor: Ministry of Health, Labor and Welfare (Health and Labor Sciences Research Grants; partial support); Grant sponsor: Ministry of Education, Culture, Sports, Science and Technology of Japan; Grant sponsor: Japan Health Sciences Foundation (Research on Publicly Essential Drugs and Medical Devices).

*Correspondence to: Harutaka Katano, Department of Pathology, National Institute of Infectious Diseases, 1-23-1 Toyama, Shinjuku, Tokyo 162-8640, Japan. E-mail: katano@nih.go.jp

Accepted 2 September 2010

DOI 10.1002/jmv.21962

Published online in Wiley Online Library (wileyonlinelibrary.com).

internal controls, theoretically 163 human viruses can be detected in a 96-well plate simultaneously. Using this system, the distribution and quantification of viruses were investigated in organ specimens from autopsies of 20 acquired immunodeficiency syndrome (AIDS) patients. In addition, clinical samples from patients with uncertain diagnoses were examined to identify the causes of infection.

MATERIALS AND METHODS

Probe–Primer Sets

A total of 163 human viruses were selected as targets (Table I). The choice of the viruses was based on their associations with human diseases, prevalence among humans, and possibility of the usages as vectors to human cells. Probe–primer sets for each virus were designed using Primer Express 2.0 (Applied Biosystems, Foster City, CA) (Supplementary Table I). Probe–primer sets published elsewhere were employed for some of the viruses. Probes and primers were synthesized by Sigma Genosys (Sigma–Aldrich, St. Louis, MO). Probes were labeled with 6-carboxyfluorescein (FAM)—6-carboxytetramethylrhodamine (TAMRA) or hexacholoro-6-carboxyfluorescein (HEX)—non-fluorescent Black Hole Quencher (BHQ)-1. Each probe–primer set was confirmed to react with at least 10 copies of a positive control plasmid containing each virus fragment, using conventional TaqMan real-time PCR (Applied Biosystems).

Establishment of Multivirus Real-Time PCR

A duplex TaqMan real-time RT-PCR system was designed to detect many viruses in a 96-well plate. Design of this system, designated as the "multivirus real-time PCR," is shown in Figure 1A. Quantitect Multiplex Probe RT-PCR kit (Qiagen, Hilden, Germany), MicroAmp Optical 96-Well Reaction Plates (Applied Biosystems), and MicroAmp Optical Adhesive Film (Applied Biosystems) were used as 2× master mix, 96-well plates, and adhesive film, respectively. Each well contains two probe–primer sets with 6-FAM- and HEX-labeled probes, allowing two viruses were to be detected in each well, and the 163 viruses listed in Table I to be detected in a 96-well plate simultaneously. A standard curve was established for nine wells of each plate (A1–A9), which contained FAM- or HEX-labeled probes and primers for green fluorescent protein and glutathione *S*-transferase genes with control plasmids at 10^1 to 10^7 copies. Thus, an approximate copy number of each virus could be calculated based on the standard curve. To use the system routinely, 2× probe–primer mix was stored in a 96-well plate at −20°C. For detection of viruses, DNA and RNA samples (50 ng per well) were added to 2× master mix with (for RNA) and without (for DNA) RT. When sufficient amounts of DNA or RNA were not obtained from clinical samples, <50 ng of DNA or RNA per well were applied in this system. Ten microliters of 2× probe–primer mix and 10 µl of 2× master mix with sample DNA (36 wells) or RNA (60 wells) were then

TABLE I. List of Target Viruses

DNA virus
Polyomavirus: JC virus, BK virus, Simian virus 40
Papillomavirus: Human papillomavirus 6, 11, 16, 18, 31, 33, 35, 39, 45, 51, 52, 56, 58, 59, 66, 68, 73
Parvovirus: Adeno-associated virus 1, 2, 3, 5; Parvovirus B19; human bocavirus; adenovirus A, B, C, D, E, F
Herpes virus: Human herpesvirus 1–8, B virus
Poxvirus: Variola virus, Monkey pox virus, Molluscum contagiosum virus
Anellovirus: Torque teno virus
Hepadnavirus: Hepatitis B virus
Other: Mimivirus
RNA virus
Filovirus: Ebola virus, Marburg virus
Bunyavirus: Crimean–Congo hemorrhagic fever virus, hemorrhagic fever with renal syndrome virus (Hantaan, Dovrava, Puumala, and Seoul), Rift valley fever virus, Sin Nombre virus
Arenavirus: Lassa virus, Junin, Guanarito, Machupo, Sabia
Togavirus: Equine encephalitis virus (Venezuelan, Eastern, and Western), Sindbis virus, Mayaro virus, Getah virus, Chikungunya virus, Rubella virus
Enterovirus: Enterovirus 68, 71; Poliovirus 1,2,3; Coxsackievirus A2, A3, A4, A5, A6, A8, A9, A10, A16, A21, A24, B1, B2, B3, B4, B5, B6; Echovirus 5, 6, 7, 9, 11, 13, 14, 16, 17, 18, 25, 30; Parechovirus 1, 3; Rhinovirus A, B; rotavirus; reovirus 1–4; Melaka virus; Colorado tick borne fever virus
Flavivirus: Dengue virus 1, 2; Japanese encephalitis virus; Murray Valley encephalitis virus; St. Louis encephalitis virus; West Nile virus; Tick-borne encephalitis virus; Yellow fever virus
Orthomyxovirus: Influenza virus A, B, C; H5N1
Paramyxovirus: Parainfluenza virus 1–3; Hendra virus; Mumps virus; Measles virus; Sendai virus; RS virus A, B; metapneumovirus; Nipah virus
Rabdovirus: Rabies virus; Lyssavirus 5, 6; Chandipura virus; Duvenhage virus
Coronavirus: Coronavirus OC43, 229E, NL63, SARS virus
Calicivirus: Sapovirus, Norwalk-like virus 1, 2
Hepatitis virus: Hepatitis A virus, Hepatitis C virus, Hepatitis D virus, Hepatitis E virus, GB virus
Retrovirus: human immunodeficiency virus 1; human T cell leukemia virus 1, 2; human endogenous retrovirus K, H, W
Other: Astrovirus, Borna disease virus

mixed in a 96-well reaction plate. Real-time RT-PCR was performed in an ABI PRISM 7900HT (Applied Biosystems) or an Mx3005P (Stratagene, La Jolla, CA). The RT-PCR conditions were 50°C for 30 min and 95°C for 15 min, followed by 40 cycles of 94°C for 15 sec, and 60°C for 1 min. Quantitative results of viruses were obtained by generating standard curves for two plasmids in the A1–A9 wells. Real-time PCR using a condition for RT-PCR (50°C for 30 min and 95°C for 15 min, followed by 40 cycles of 94°C for 15 sec and 60°C for 1 min) had similar sensitivity to real-time PCR using usual DNA conditions (95°C for 5 min, followed by 40 cycles of 94°C for 15 sec and 60°C for 1 min) in the detection for some DNA viruses (Supplementary Fig. 1A). In addition, the duplex real-time PCR using Quantitect Multiplex Probe RT-PCR kit (Qiagen) had similar sensitivity to single real-time PCR procedures using Quantitect Probe RT-PCR kit (Qiagen) in several probe–primer sets (Supplementary Fig. 1B).

Gene Expression Image

A gene expression image was produced with TreeView and Cluster software by Michael Eisen, University of California at Berkeley (http://rana.lbl.gov/EisenSoftware.htm) [Eisen et al., 1998].

Determination of the Positivity and Copy Numbers of Viruses

The positivity and virus titer of all positive samples were confirmed with individual standard real-time (RT-) PCR systems using the same probe–primer sets. Virus DNA copy numbers per cell were calculated by dividing virus DNA copy numbers by half of beta-actin copy numbers, since each cell has two copies of DNA in two alleles [Asahi-Ozaki et al., 2006].

Patients and Samples

The study protocol was approved by the Institutional Review Board, National Institute of Infectious Diseases, Japan (Approval No. 156). Tissues were taken at autopsy from various organs of 20 patients with AIDS. All tissues were frozen immediately, and stored at −80°C. The clinical information of the patients is summarized in Table II. A total of 19 patients were male. The mean age of the patients was 41.8 years (range: 19–67 years), and the mean of CD4 counts was 17 cells/μl (range: 0–241). Risk factors for HIV infection in the patients were men who had sex with men (10), heterosexuality (5), and hemophilia (5). At least seven patients had lymphoma, and two had Kaposi's sarcoma. No patients received highly active anti-retroviral therapy (HAART). In addition, 40 clinical samples from patients with uncertain diagnoses were investigated (Table III). These clinical samples were sent to our department for virus diagnosis. Informed consents were obtained by the clinical doctors. Positive control

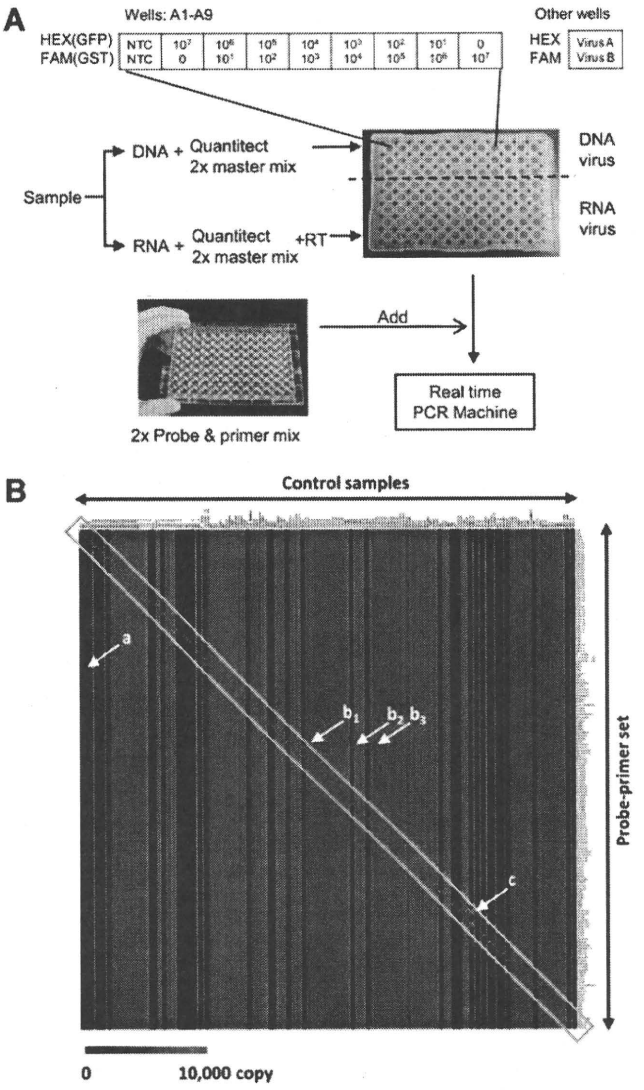

Fig. 1. Establishment and validation of multivirus real-time PCR. **A**: Procedure of the multivirus real-time PCR system. DNA sample was mixed with Quantitect 2× master mix, and RNA sample was mixed with Quantitect 2× master mix and reverse transcriptase (RT) mix. These mixtures were poured into each well in a 96-well plate at 10 μl per well. Ten microliters of 2× probe and primer mix were then added to each well in a premixed 96-well plate. Finally, the virus genes were amplified and detected in a real-time PCR machine for 2 hr. **B**: Validation of the multivirus real-time PCR. A gene expression image by TreeView software based on the results of the multivirus real-time PCR for control samples is shown. A horizontal line shows each probe–primer set and a vertical line is one sample of positive control. Gray vertical lines indicate no sample. A scale bar indicates copy number of color. A green box indicates specific reactions of target positive controls in specific probe–primer sets. Arrows of (a–c) also show specific signals. The arrow (a) shows positive signal for TTV in a brain sample with both JCV and TTV infection. The arrows (b1–3) show that a probe–primer set for pan-enterovirus reacted with poliovirus (b1), Coxsackievirus B3 (b2), and Echovirus 6 (b3) positive samples. The arrow (c) shows that a probe–primer set for influenza virus A reacted with H5N1 influenza virus. Details of positive controls were listed in Supplementary Table II.

DNA or RNA samples extracted from virus-infected cells or tissues were kindly provided by many researchers in National Institute of Infectious Diseases (Supplementary Table II).

TABLE II. Clinical Information and Detected Viruses in AIDS Autopsies

Case no.	Age	Sex	Risk factor	Complications	CD4[a]	Detected viruses by multivirus real-time PCR
1	49	M	MSM	PCP, aspergillus	NT	TTV, HBV, HERV-H
2	37	M	MSM	CMV, toxoplasma, PCP	NT	HSV-1, CMV, TTV, HIV-1, HERV-H
3	29	M	Drug	PCP	1	JCV, Adv-B, HSV-1, EBV, CMV, HHV-6, HHV-7, TTV, HBV, HIV-1, HERV-H
4	37	M	Blood product	MAC, CMV	1	EBV, CMV, HHV-6, TTV, HIV-1, HERV-H
5	43	M	Heterosexual	ML, CMV, cryptococcus	5	B19, Adv-A, EBV, CMV, HHV-6, TTV, HIV-1, HERV-H
6	54	M	MSM	CMV	NT	EBV, CMV, HHV-6, TTV, HBV, HIV-1, HERV-H
7	33	M	MSM	CMV	4	B19, CMV, HHV-6, TTV, HIV-1, HERV-H
8	47	M	MSM	HIV-encephalitis, KS, ML	1	BKV, CMV, HHV-6, TTV, HIV-1, HCV
9	35	M	Blood product	CMV	1	B19, CMV, TTV, HIV-1, HERV-H
10	27	F	Heterosexual	ML, MAC, CMV	3	BKV, EBV, CMV, TTV, HIV-1, HERV-H
11	50	M	MSM	HIV-encephalitis, ML, cryptococcus, CMV	0	B19, CMV, HHV-6, TTV, HIV-1, HERV-H
12	19	M	Blood product	HIV-encephalitis	2	BKV, TTV, HIV-1, HERV-H
13	26	M	Blood product	PML	3	JCV, BKV, B19, Adv-B, EBV, HHV-6, HHV-7, TTV, Echo6, HCV, HERV-H
14	67	M	MSM	ML	241	JCV, CMV, HHV-6, TTV, HIV-1, HERV-H
15	62	M	MSM	CMV, PCP	4	AAV-2, B19, EBV, CMV, HHV-6, TTV, HIV-1, HERV-H
16	28	M	Blood product	CMV, MAC	3	JCV, BKV, B19, CMV, HHV-7, TTV, HBV, HIV-1, HERV-H
17	46	M	Heterosexual	ML, aspergillus, CMV	5	BKV, AAV-2, B19, Adv-D, EBV, CMV, HHV-6, TTV, RSV-B, HIV-1
18	47	M	MSM	PEL, CMV	7	JCV, B19, EBV, CMV, HHV-6, HHV-8, TTV, HIV-1, HERV-K, HERV-H
19	60	M	MSM	ML, CMV, KS	1	B19, CMV, TTV, HIV-1, HERV-H
20	40	M	Heterosexual	CMV	NT	BKV, AAV-2, CMV, HHV-6, HHV-7, TTV, HBV, HERV-H

AAV, adeno-associated virus; Adv, adenovirus; B19, parvovirus B19; BKV, BK virus; CMV, cytomegalovirus; EBV, Epstein–Barr virus; HBV, hepatitis B virus; HCV, hepatitis C virus; HERV, human endogenous retrovirus; HHV, human herpesvirus; HIV-1, human immunodeficiency virus 1; HSV, herpes simplex virus; JCV, JC virus; KS, Kaposi's sarcoma; MAC, mycobacterium avium-intracellulare complex; ML, malignant lymphoma; MSM, Men who have sex with men; NT, not tested; PCP, Pneumocystis pneumonia; PML, progressive multifocal leukoencephalopathy; RSV, respiratory syncytial virus; TTV, Torque teno virus.
[a]CD4 counts per μl.

DNA and RNA Extraction

Nucleic acid extraction methods differed according to the type of samples. Each frozen tissue sample was divided in two, one part for DNA extraction and another for RNA extraction. For DNA extraction, the samples were homogenized with Multi-Beads Shocker (Yasui Kikai, Tokyo, Japan) in TEN buffer (10 mM Tris–HCl, pH 8.0, 1 mM EDTA, pH 8.0, and 100 mM NaCl) with 100 ng/ml proteinase K and 0.1% sodium dodecyl sulfate. DNA was extracted from the homogenized tissues using the phenol–chloroform method. Total RNA was extracted from frozen tissues using Isogen (Nippon Gene, Tokyo, Japan). The samples were homogenized in the Isogen with Multi-Beads Shocker, and the extraction was performed according to the manufacturer's instructions. For small samples including tissue biopsy, blood, serum and cerebral fluid, both DNA and RNA were extracted simultaneously with All Prep Kit (Qiagen). All RNA samples were treated with DNase (Turbo DNA-Free, Ambion, Austin, TX) for 20 min according to the manufacturer's instructions.

RESULTS

Validation of Multivirus Real-Time PCR

To validate the sensitivity and specificity of each probe and primer set used in the system, DNA or RNA samples

TABLE III. Identification of Pathogenic Virus in Clinical Samples From Patients With Uncertain Diagnoses

Patients	n	Samples	Identified pathogens (cases)
Hepatitis	9	Liver biopsy	Parvovirus B19 (2), HHV-6 (3), TTV (2)
Encephalitis	11	Brain biopsy, serum, cerebral fluids	HSV-1 (2), HHV-6 (1), parechovirus 3 (1)
Myocarditis	6	Heart autopsy	Parvovirus B19 (1), TTV (2)
Sudden death	4	Blood, serum	TTV (1)
Other	10	Tissue, blood, serum	Parvovirus B19 (1), EBV (1), CMV (1), HHV-7 (1), TTV (2)
Total	40	—	—

Etiological viruses in the cases are underlined.

extracted from virus-infected cells, supernatants, body fluids, or tissues were examined in this multivirus real-time PCR system (Supplementary Table II). Each probe and primer set amplified a gene fragment of target virus specifically (Fig. 1B and Supplementary Table II). When using supernatants of virus-infected cells, the reactions were specific. Some samples of supernatants were positive for two or three viruses, because the target virus belonged to several categories. For example, the RNA sample extracted from supernatants of H5N1 influenza virus-infected cells was positive in the wells with probe and primer sets for both H5N1 influenza virus and influenza-A virus. Some clinical samples, such as pathological samples and body fluids, were positive for other viruses as well as target viruses because of the presence of such viruses in the samples (Supplementary Table II and Fig. 1B, arrow (a)). Although not all positive control samples could be collected, the results confirmed the adequate specificity of each probe–primer set for its target virus for virus screening. The multivirus real-time PCR system also detects human internal control genes such as glyceraldehyde-3-phosphate dehydrogenase (GAPDH, DNA, and mRNA), beta-actin (DNA), and beta-2-microgloblin (mRNA) (Supplementary Tables I and II). It is known that certain specimen such as serum may have inhibitory effects on PCR [Vandenvelde et al., 1993; Willems et al., 1993]. Copy numbers of internal controls would be informative to know cell numbers and inhibitory effect by the sample.

Detection of Viruses in AIDS Autopsies

Using the multivirus real-time PCR, the presence of viruses was investigated in 20 AIDS autopsies. The multivirus real-time PCR detected 15 DNA viruses: JC virus (JCV), BK virus (BKV), adeno-associated virus (AAV)-2, parvovirus B19, three subgroups of adenovirus (A, B, and D), herpes simplex virus 1 (HSV-1), Epstein–Barr virus (EBV), cytomegalovirus (CMV), human herpesvirus (HHV)-6, -7, -8, TT virus (TTV), and

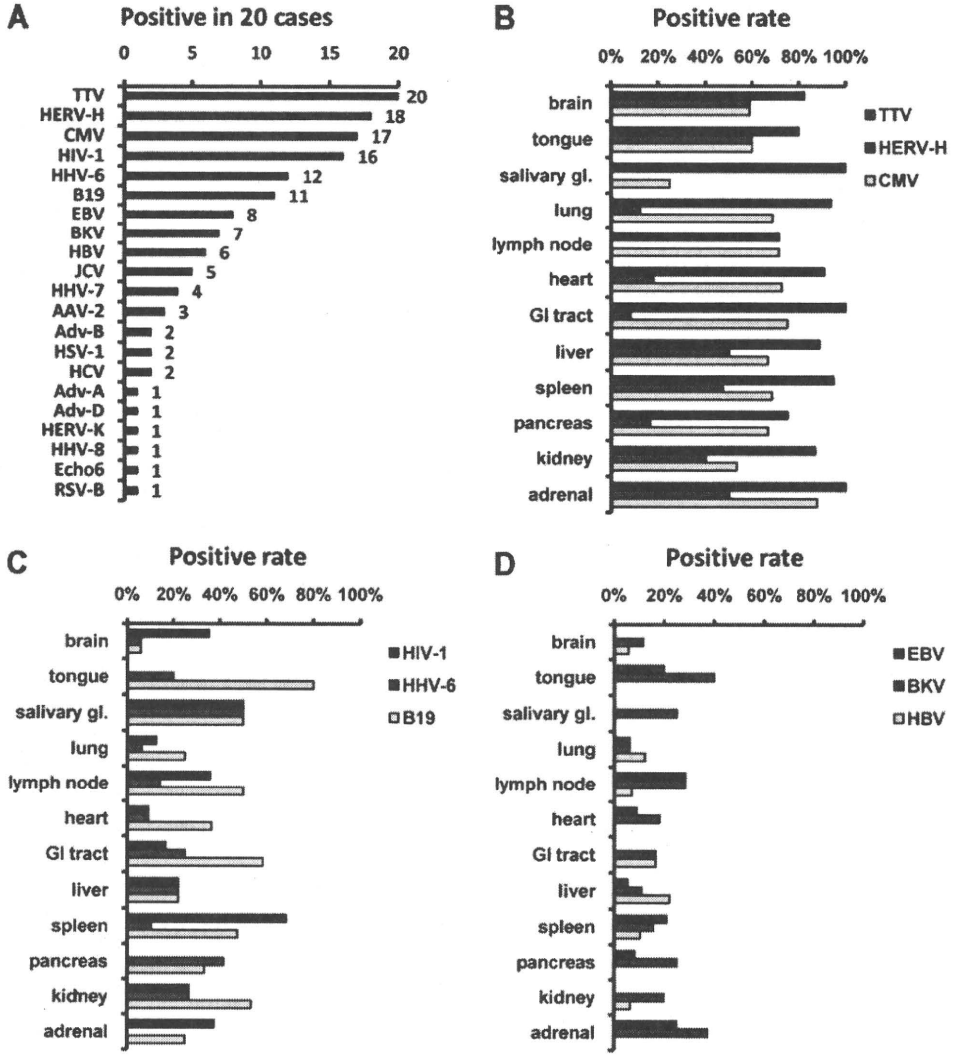

Fig. 2. Viruses detected in autopsied organs of AIDS patients. **A**: Positive number of each virus in the 20 cases of AIDS autopsy. **B–D**: Positive rates of CMV, HIV-1, and HHV-6 in organs. GI, gastrointestinal.

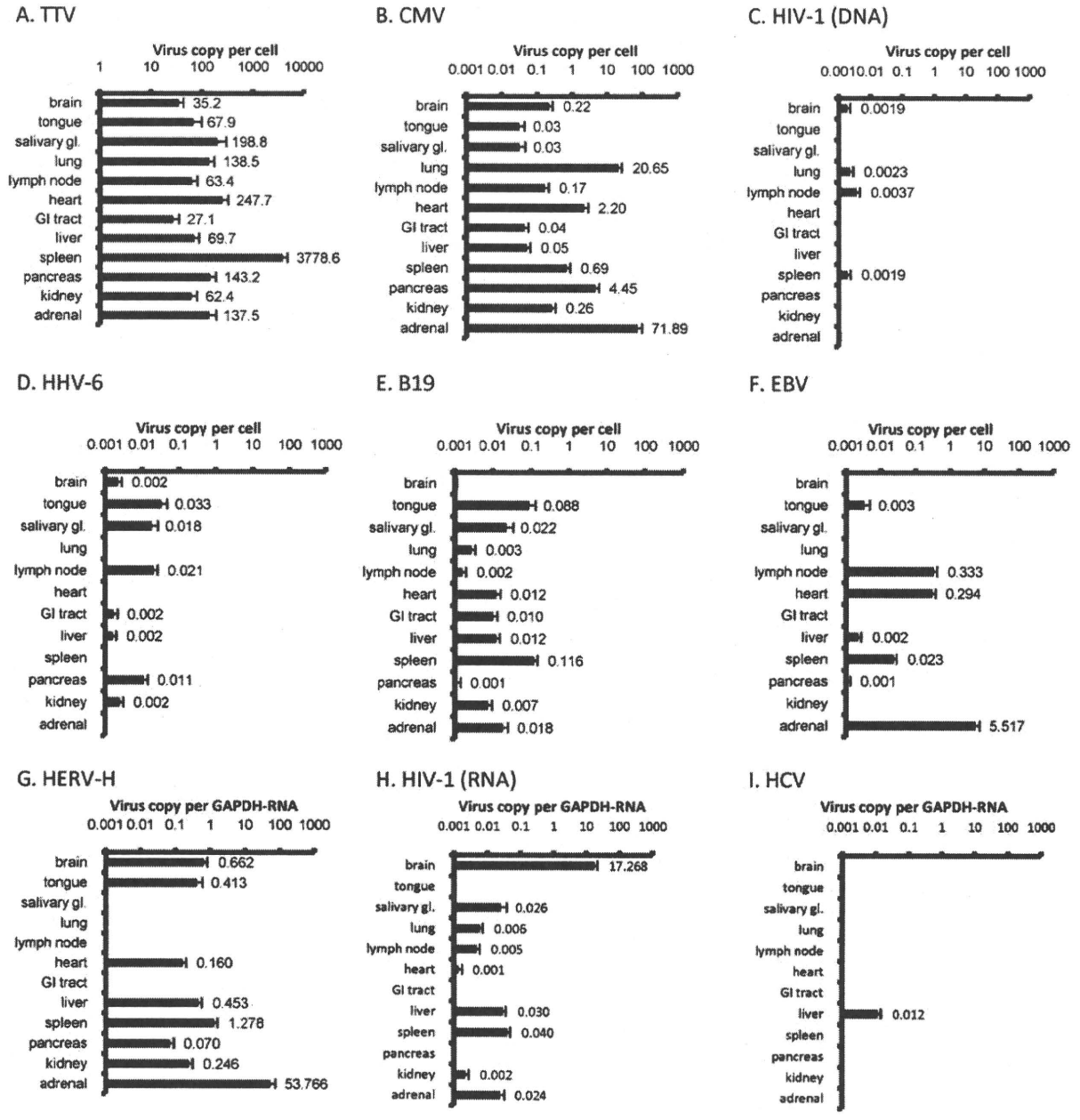

Fig. 3. Mean values of virus copy numbers in organs. Mean of copy numbers per cells are shown in DNA samples (**A–F**). Mean ratios of virus copy number per hGAPDH-RNA copy number are shown in RNA samples (**G–I**). Error bars show standard errors. One brain sample contained HIV-associated encephalopathy (C,H), and one of the heart and adrenal sample contained EBV-associated lymphoma (F).

hepatitis B virus (HBV). It also detected six RNA viruses: echovirus 6, respiratory syncytial (RS) virus type B, hepatitis C virus (HCV), HIV-1, and human endogenous retrovirus (HERV)-H and -K, in 20 cases of AIDS autopsies (Fig. 2). A few other viruses were detected at low copies in some samples, but additional individual standard real-time (RT-) PCR systems using the same probe–primer sets showed negative results, indicating that they were false positive. Although HIV-1 infections were confirmed clinically in all the patients, HIV-1 was not detected in four of the autopsy cases, even using both DNA and RNA samples. TTV, HERV-H, CMV, HIV, HHV-6, parvovirus B19, EBV, BKV, and HBV were detected in many organs, suggesting broad distribution (Fig. 2B–D). On the other hand, the positive rate of each virus differed among organs. CMV was detected most frequently in the adrenal gland, but HIV-1 was most common in the spleen, HHV-6 in the salivary gland, and HBV in the liver.

The multivirus real-time PCR also revealed copy numbers of each virus in AIDS autopsy (Fig. 3). High numbers of TTV copies were detected frequently in various organs without any symptoms, suggesting a ubiquitous distribution in the samples and no associa-

tion with any specific diseases (Fig. 3A). High numbers of CMV copies were detected in adrenal gland, lung, and pancreas (Fig. 3B). To confirm the results of the real-time PCR, CMV positivity was investigated using inclusion bodies in the pathological samples. Inclusion bodies of CMV were detected frequently in the adrenal gland, pancreas, and lung of AIDS autopsy cases (Supplementary Fig. 2). These results correlated with those of the real-time PCR. HHV-6 and parvovirus B19 showed low copy numbers in all the organs tested (Fig. 3D,E). High numbers of EBV copies were detected in the heart and adrenal gland, as well as lymph node and spleen (Fig. 3F). However, the heart and adrenal samples included lesions of EBV-associated lymphomas. Thus, EBV was detected in the lymphomas in those samples. The lymphomas in adrenal glands also included high numbers of HERV-H copies, affecting the results of HERV-H copy numbers in adrenal glands (Fig. 3G). High numbers of HIV-1-RNA copies, but not HIV-1-DNA, were also found in the brain of one case with HIV-1 encephalopathy (Fig. 3C,H). HCV was detected only in the liver of two patients (Fig. 3I).

Identification of Virus in Clinical Samples From Patients With Uncertain Diagnoses

Using the multivirus real-time PCR, clinical samples from 40 patients with uncertain diagnoses were examined to identify their causes of infection (Table III). The multivirus real-time PCR system identified HSV-1, HHV-6, or parechovirus 3 as a possible cause of infection in 4 out of 11 patients with encephalitis. HSV-1 was identified in brain biopsy tissues from two patients with encephalitis. A high copy number of HHV-6 was detected in the serum of a patient (1.5×10^7 copies/ml in the serum). In another patient, parechovirus 3 were detected in cerebral fluids. The presence of these viruses in the samples was confirmed by individual real-time PCR specific for each virus, and conventional (RT-) PCR. Clinical manifestations of these four patients were compatible with the virus infections. In addition, 29 samples from patients with other diseases such as myocarditis, hepatitis, and sudden death were examined. Parvovirus B19, EBV, CMV, HHV-6, HHV-7, and TTV were detected in the samples; however, the titers of these viruses were low. In addition, immunohistochemistry and in situ hybridization could not detect the viruses in the samples. It was therefore concluded that these viruses were not the causes of diseases in the cases.

DISCUSSION

In the present study, a new real-time PCR system was developed, designated as the "multivirus real-time PCR," that had the potential to detect 163 viruses simultaneously. This multivirus real-time PCR can detect 47 DNA viruses and 116 RNA viruses on a 96-well plate theoretically. This system revealed the anatomical distributions of human pathogenic viruses in AIDS autopsy cases. In addition, viruses were identified in four cases of encephalitis as the cause of infection. This multivirus real-time PCR system could be a useful technique for detection of virus in specimens from patients with uncertain diagnoses.

Real-time PCR is a sensitive detection system for the diagnosis of virus infection. TaqMan PCR has a high specificity compared with other systems because of its specific fluorescence probes. In addition, recent multiplex fluorescence technology is able to detect several genes in each tube without non-specific cross-reactions. Since one-step real-time RT-PCR employs specific primers as RT primers, with targets shorter than 100 bp, this system can detect short fragments of RNA viruses specifically with high sensitivity. The sensitivity and specificity of this system are equivalent to those of standard real-time PCR systems (Supplementary Fig. 1), and its sensitivity would be much higher than in microarray systems. In addition, the multivirus real-time PCR system requires only 5 μg each of DNA and RNA for detecting 163 viruses.

One disadvantage of this system is cost. To establish this system, 176 probe–primer sets should be prepared. Moreover, about 1 ml of Quantitect 2× master mix was used in single reaction of 96-well plate, which costs about 25,000 yen (approximately 263 U.S. dollars; containing probe–primer sets: ¥36 × 176 sets = ¥6,336, Quantitect 2× master mix: ¥16,000, filtered tips, 96-well reaction plate and seal: ¥2,664) per sample in a 96-well plate reaction to test. However, once the system is established, the procedure is very easy and takes 3 hr to obtain the results. Thus, the newly developed multivirus real-time PCR could be a useful tool for detecting pathogens in specimens from patients with uncertain diagnoses.

There is little current information about quantification of pathogenic viruses in immunocompromised hosts. Chen and Hudnall [2006] described anatomical mapping of herpes viruses in eight autopsy cases, including two AIDS cases. The multivirus real-time PCR showed that 21 of the 163 probe–primer sets for virus produced positive reactions in AIDS autopsy samples. Many RNA viruses were negative in all cases. Although the low detection rate of RNA viruses might be associated with the quality of extracted RNA, these results suggest that the AIDS patients in the present study were infected with limited types of viruses. TTV and HHV-6 were detected frequently in AIDS autopsy samples and some clinical samples. TTV was identified from a hepatitis patient as a hepatitis-associated virus [Nishizawa et al., 1997]. However, TTV, a ubiquitous virus, was shown to be present in various tissues [Okamoto, 2009]. Although TTV titers were relatively high compared with those of other viruses, broad TTV distribution suggests that it is not associated with specific diseases in immunocompromised hosts. HHV-6 is another ubiquitous virus with which almost 100% of adults are infected. Primary infection of HHV-6 causes exanthema subitum in children [Yamanishi et al., 1988]. Reactivation of HHV-6 may cause hepatitis, pneumonia, and encephalitis in immunocompromised hosts, such as

transplant patients [Ljungman, 2002]. The average number of HHV-6 copies in the HHV-6-positive samples in AIDS autopsy was 0.008 copies per cell, suggesting low numbers of HHV-6 copies in the organs. On the other hand, HHV-6 was identified as a possible cause of infection in a clinical case of encephalitis because of extremely high numbers of copies in the serum and clinical manifestations [Ogata et al., 2010]. Thus, a virus's copy number is important information to estimate its etiology. CMV was frequently detected in AIDS autopsy samples by the multivirus real-time PCR system. High CMV copy numbers in the adrenal gland, pancreas and lung were associated with the occurrence of CMV-associated adrenitis, pancreatitis, and pneumonia. CMV was detected frequently in the adrenal gland [Pulakhandam and Dincsoy, 1990]. The results of CMV detection in multivirus real-time PCR were correlated highly with the frequency of CMV inclusion bodies on the slides, suggesting that the occurrence of CMV-associated diseases is associated with virus titers of CMV in organs.

The multivirus real-time PCR failed to detect HIV-1 DNA or RNA in 4 cases out of 20 AIDS autopsies. There are several possible explanations for these results. Although none of the patients received HAART, HIV-1 titers always change in AIDS patients [Ho et al., 1989]; the autopsy samples might have had insufficient HIV-1 titers for detection by real-time PCR. Also, the probe and primers used in this system might not detect the HIV-1 because of mutations in the target regions. Mutations in HIV-1 occur so frequently that it is difficult to detect HIV-1 using one or two probe–primer sets [Desire et al., 2001; Yun et al., 2002].

Consequently, a multivirus real-time PCR system with the potential to detect 163 viruses simultaneously has been established in the present study. Although the system has some disadvantages with regard to cost and procedure, it will be a powerful tool for virus screening of clinical samples in laboratories. Since it is relatively easy to change probe–primer sets in the 96-well plate, it is possible for this system to change detectable viruses, implying that a new system detecting new viruses can be established quickly. Future refinement of its operation, such as higher throughput and microfluid techniques, may resolve the disadvantages of this system.

ACKNOWLEDGMENTS

We thank Mr. Kouta Sakamoto and Ms. Yuko Sato for technical assistant and Dr. Tadahito Kanda, Dr. Seiichiro Mori, Dr. Takato Odagiri, Dr. Atsushi Kato, Dr. Katsuhiro Komase, Dr. Fumihiro Taguchi, Dr. Kei Numazaki, Dr. Shigeru Morikawa, Dr. Tomohiko Takasaki, Dr. Naoki Inoue, Dr. Tetsuro Suzuki, Dr. Naokazu Takeda, Dr. Tetsuo Yoneyama, Dr. Hiroyuki Shimizu, Dr. Haruko Shirato, Dr. Toshihiko Matsukura, Dr. Asato Kojima, Dr. Hidehiro Takahashi, Dr. Kenzo Tokunaga, Dr. Michiko Tanaka, Dr. Kiyoko Ogawa-Goto, and Dr. Yasuko Asahi-Ozaki of the National Institute of Infectious Diseases for providing positive controls for RNA or DNA extracted from virus-infected cells.

REFERENCES

Asahi-Ozaki Y, Sato Y, Kanno T, Sata T, Katano H. 2006. Quantitative analysis of Kaposi sarcoma-associated herpesvirus (KSHV) in KSHV-associated diseases. J Infect Dis 193:773–782.

Bellau-Pujol S, Vabret A, Legrand L, Dina J, Gouarin S, Petitjean-Lecherbonnier J, Pozzetto B, Ginevra C, Freymuth F. 2005. Development of three multiplex RT-PCR assays for the detection of 12 respiratory RNA viruses. J Virol Methods 126:53–63.

Chen T, Hudnall SD. 2006. Anatomical mapping of human herpesvirus reservoirs of infection. Mod Pathol 19:726–737.

Desire N, Dehee A, Schneider V, Jacomet C, Goujon C, Girard PM, Rozenbaum W, Nicolas JC. 2001. Quantification of human immunodeficiency virus type 1 proviral load by a TaqMan real-time PCR assay. J Clin Microbiol 39:1303–1310.

Eisen MB, Spellman PT, Brown PO, Botstein D. 1998. Cluster analysis and display of genome-wide expression patterns. Proc Natl Acad Sci USA 95:14863–14868.

Ho DD, Moudgil T, Alam M. 1989. Quantitation of human immunodeficiency virus type 1 in the blood of infected persons. N Engl J Med 321:1621–1625.

Li H, McCormac MA, Estes RW, Sefers SE, Dare RK, Chappell JD, Erdman DD, Wright PF, Tang YW. 2007. Simultaneous detection and high-throughput identification of a panel of RNA viruses causing respiratory tract infections. J Clin Microbiol 45:2105–2109.

Ljungman P. 2002. Beta-herpesvirus challenges in the transplant recipient. J Infect Dis 186:S99–S109.

Mahony J, Chong S, Merante F, Yaghoubian S, Sinha T, Lisle C, Janeczko R. 2007. Development of a respiratory virus panel test for detection of twenty human respiratory viruses by use of multiplex PCR and a fluid microbead-based assay. J Clin Microbiol 45:2965–2970.

Molenkamp R, van der Ham A, Schinkel J, Beld M. 2007. Simultaneous detection of five different DNA targets by real-time Taqman PCR using the Roche LightCycler480: Application in viral molecular diagnostics. J Virol Methods 141:205–211.

Nishizawa T, Okamoto H, Konishi K, Yoshizawa H, Miyakawa Y, Mayumi M. 1997. A novel DNA virus (TTV) associated with elevated transaminase levels in posttransfusion hepatitis of unknown etiology. Biochem Biophys Res Commun 241:92–97.

Nolte FS, Marshall DJ, Rasberry C, Schievelbein S, Banks GG, Storch GA, Arens MQ, Buller RS, Prudent JR. 2007. MultiCode-PLx system for multiplexed detection of seventeen respiratory viruses. J Clin Microbiol 45:2779–2786.

Ogata M, Satou T, Kawano R, Takakura S, Goto K, Ikewaki J, Kohno K, Ikebe T, Ando T, Miyazaki Y, Ohtsuka E, Saburi Y, Saikawa T, Kadota J. 2010. Correlations of HHV-6 viral load and plasma IL-6 concentration with HHV-6 encephalitis in allogeneic stem cell transplant recipients. Bone Marrow Transplant 45:129–136.

Okamoto H. 2009. History of discoveries and pathogenicity of TT viruses. Curr Top Microbiol Immunol 331:1–20.

Pulakhandam U, Dincsoy HP. 1990. Cytomegaloviral adrenalitis and adrenal insufficiency in AIDS. Am J Clin Pathol 93:651–656.

Storch GA. 2000. Diagnostic virology. Clin Infect Dis 31:739–751.

van de Pol AC, van Loon AM, Wolfs TF, Jansen NJ, Nijhuis M, Breteler EK, Schuurman R, Rossen JW. 2007. Increased detection of respiratory syncytial virus, influenza viruses, parainfluenza viruses, and adenoviruses with real-time PCR in samples from patients with respiratory symptoms. J Clin Microbiol 45:2260–2262.

Vandenvelde C, Scheen R, Defoor M, Duys M, Dumon J, Van Beers D. 1993. Suppression of the inhibitory effect of denatured albumin on the polymerase chain reaction by sodium octanoate: Application to routine clinical detection of hepatitis B virus at its infectivity threshold in serum. J Virol Methods 42:251–263.

Vet JA, Majithia AR, Marras SA, Tyagi S, Dube S, Poiesz BJ, Kramer FR. 1999. Multiplex detection of four pathogenic retroviruses using molecular beacons. Proc Natl Acad Sci USA 96:6394–6399.

Wada K, Mizoguchi S, Ito Y, Kawada J, Yamauchi Y, Morishima T, Nishiyama Y, Kimura H. 2009. Multiplex real-time PCR for the simultaneous detection of herpes simplex virus, human herpesvirus 6, and human herpesvirus 7. Microbiol Immunol 53:22–29.

Wang D, Coscoy L, Zylberberg M, Avila PC, Boushey HA, Ganem D, DeRisi JL. 2002. Microarray-based detection and genotyping of viral pathogens. Proc Natl Acad Sci USA 99:15687–15692.

Willems M, Moshage H, Nevens F, Fevery J, Yap SH. 1993. Plasma collected from heparinized blood is not suitable for HCV-RNA detection by conventional RT-PCR assay. J Virol Methods 42: 127–130.

Yamanishi K, Okuno T, Shiraki K, Takahashi M, Kondo T, Asano Y, Kurata T. 1988. Identification of human herpesvirus-6 as a causal agent for exanthem subitum. Lancet 1:1065–1067.

Yun Z, Fredriksson E, Sonnerborg A. 2002. Quantification of human immunodeficiency virus type 1 proviral DNA by the TaqMan real-time PCR assay. J Clin Microbiol 40:3883–3884.